COMPARISON OF FATIGUE CRACK GROWTH RATE IN NATURALLY AGED AND NON-AGED, WELDED AND NON-WELDED AISI AL-2219-T87

In partial fulfillment of requirement for the degree in

M.S Mechanical Engineering

Author

Engr. Muhammad Mudasir Ijaz
32-FET-MSME-F14

Supervisor
Dr. Engr. Saeed Badshah
Associate Professor

DEPARTMENT OF MECHANICAL ENGINEERING
FACULTY OF MECHANICAL AND AERONAUTICAL ENGINEERING
INTERNATIONAL ISLAMIC UNIVERSITY ISLAMABAD

Dec 2017

MS
620·1126.
I JC

Fatigue (Materials)

Fracture mechanics.

COMPARISON OF FATIGUE CRACK GROWTH RATE IN NATURALLY AGED AND NON-AGED, WELDED AND NON-WELDED AISI AL-2219-T87

Author

Muhammad Mudasir Ijaz

32-FET-MSME-F14

A thesis submitted in partial fulfillment of the requirements for the degree of

M.S in Mechanical Engineering

Thesis Supervisor

Dr. Engr. Saeed Badshah

Associate Professor, Department of Mechanical Engineering, IIU Islamabad

External Examiner Signature: _____
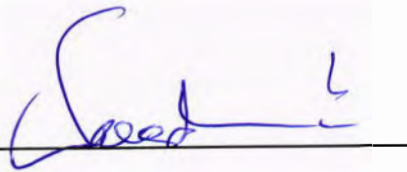
Thesis Supervisor Signature: _____

Certificate of Approval

This is to certify that the work contained in this thesis entitled, **"Comparison of Fatigue Crack Growth Rate in Naturally Aged and Non-Aged, Welded and Non-Welded AISI Al-2219"** was carried out by **Muhammad Mudasir Ijaz, Registration # 32/FET/MSME/F14,** is fully adequate in scope and quality for the degree of MS Mechanical Engineering.
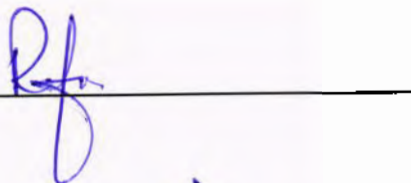
Viva Voice Committee

Supervisor

Dr. Engr. Saeed Badshah
Associate Professor
DME, FET, IIU Islamabad_____

Internal Examiner

Dr. Rafi Ullah Khan
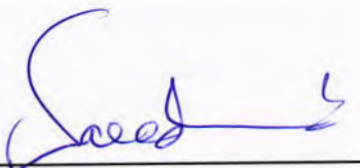Assistant Professor
DME, FET, IIU Islamabad_____

External Examiner
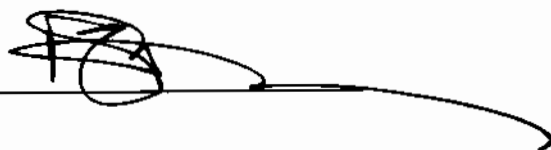
Dr. Ameer Badshah
DCM
NESCOM, Islamabad_____

Chairman

DME, FET, IIU Islamabad_____

Dean FET/ IIU Islamabad_____

Prof. Dr. Engr. Muhammad Amir

Declaration

I certify that research work titled **"Comparison of Fatigue Crack Growth Rate in naturally aged and non-aged, welded and non-welded AISI Al-2219-T87"** is my individual effort. The work has not been presented anywhere else for evaluation. Material that has been used from other sources, is properly recognized / cited.

<div align="right">

Muhammad Mudasir Ijaz

32-FET-MSME-F14

</div>

Dedication

Although this is not enough and this sentence cannot define what I feel for them, I dedicate this research thesis to my beloved Prophet Muhammad (P.B.U.H), parents and my grandmother whose prayers and support made me achieve this milestone. They believed in me and always encouraged me at every step of life.

Acknowledgements

Abstract

The effect of natural ageing on fatigue crack growth rate (FCGR) of welded and non-welded compact tension (CT) specimens (AA2219-T87) has been studied on MTS 810. Results thus obtained are compared with already published data of same specimens without ageing. AA2319 has been used as a filler material during TIG welding. Fatigue testing has been performed as per ASTM E399 standard which provides the data for crack length in CT specimen. Standard procedure for testing is being adopted to draw plot of stress intensity factor (ΔK) vs crack ratio (a/W) for different value of crack length in base metal and welded zone. Optical method has been used to obtain the crack lengths and values are calculated from CMOD in accordance with ASTM E399 standard. Paris curves are generated for both welded and non-welded specimens and compared to study the effect of natural ageing (NA) on FCGR and are compared with non-aged specimens.

Table of contents

List of Figures

List of Table

Symbols & Abbreviations

Symbols	
da/dN	Crack propagation rate with cubic spline smoothing
$\Delta a/\Delta N$	Crack propagation rate without smoothing
C	Intercept of Paris law
m	Slope of Paris law
B	Thickness of specimen
a/W	Crack length to width ratio
H/W	Specimen height to width ratio
K_I	Mode I stress intensity factor
K_{IC}	Plane strain critical stress intensity factor
K_C	Critical stress intensity factor
ΔK	Stress intensity factor range
ΔK_{eff}	Effective stress intensity factor range
R	Load ratio
N_f	Endurance cycles

Abbreviations	
LEFM	Linear elastic fracture mechanics
EPFM	Elastic plastic fracture mechanics
FCG	Fatigue crack growth
FCGR	Fatigue crack growth rate
LSY	Large scale yielding
SSY	Small scale yielding
SIF	Stress intensity factor
TIG	Tungsten inert gas
BM	Base metal
HAZ	Heat affected zone
WNZ	Weld nugget zone
C(T)	Compact Tension
ASTM	American society of testing material
GPZ	Guinier-preston zone

1 *Introduction*

1.1 Objective

The main objective of our research work is to find out the effect of natural aging on TIG welded and non-welded AA2219-T87 alloy. AA2219 is an alloy of aluminum with Cu as its main component. It has wide range of applications in the aerospace and automotive industry. TIG welding with AA2219 alloy is found to be the best welding technique so far. The filler material employed in this research is AA2239 which is the best combination with it. When the parts are to be kept for a three to four month, than it is necessary to find out the changing that may take place due to natural aging. Our research is to find out the fatigue crack propagation rate of naturally aged aluminum alloy and compare its results with already published data of same material without natural aging.

1.2 Motivation

The material being used in our research is AA2219 because of its extensive application in aerospace and automotive industry. Previously the work had been performed on fresh specimen and the fatigue behavior was the main subject of investigation in that research. Similarly, the previous work mainly describes the fatigue crack growth behavior and its effect by employing different welding techniques. No specific work had been done on the natural aging of TIG welded material. Our work will not only investigate the fatigue crack behavior on aged specimen but also compare them with the already published data on the same specimen in pre-aged condition.

1.3 Organization of Thesis

As per the mandatory requirements of the thesis, it has been compiled in the form of chapters.

Chapter 1: It includes the introduction, objective and the literature review of the research work which is being carried out by the previous researchers.

Chapter 2: The details of experimental work, machines and all procedures are included in this chapter.

Chapter 3: Microstructure of Al2219-T87 before and after natural aging, welded and non-welded is being discussed in it.

Chapter 4: Covers the microstructure behavior of base metal & TIG weldment zones, before and after aging, on the bases of Al-Cu phase diagram.

Chapter 5: Contains before and after aging results.

Chapter 6: Contains before and after aging conclusions with Future Recommendations.

1.4 Literature Review

In the design of engineering components, it is essential to estimate its fatigue life. To avoid such unexpected failures, a comprehensive study of fatigue failure analysis has been done[1].

The main approaches used in fatigue crack modeling are as:

1.   Fracture Mechanics Approach

2.   Strain Based

3.   Stress based (S-N Curve)

Above these approaches, fracture mechanics approach is mainly used in understanding the fatigue failures.

It is conventional to check the fatigue life of notched specimens. During the investigation, it is observed that there are mainly two types of effects which are associated with notches i.e. statistical size and geometrical size effect[1]. Statistical size effect is assessed with the maximum depth of already initiated crack in subjected material if the variation in stresses in effective area is very high. In other words, it is tried to describe that when specimen is undergoing varying cyclic load, there will be large number of micro cracks generated in its whole volume. After that crack branches are created and these may totally different on both side of whole thickness [3].

Fig 1.1 Welding application

The resistance to fatigue crack propagation (FCP) is badly damaged by artificial aging, which is very clear from the relationship commonly used is between stress intensity factor K (K_{max} - K_{min}) and crack growth rate (da/dn). This deprivation highly limits the aluminum alloys such as AA2219 to naturally age when used in aircrafts and automotive application in a tension dominated area which require fatigue damage tolerance.[4][5, 6]. The artificially aged and T8 tempered have higher strength and is beneficial for use without the loss of fatigue tolerance. The mechanism of microstructure effect on the crack growth , especially in the 7xxx series which is being studied more intensively, involves many localized and interactive processes of crack tip including: (a) ecological contact, (b)deflection and path tortuosity, (c) coarseness and corrosion product-induced closure[7].The closure mechanism, at which the artificial aging degrades the fatigue crack propagation resistance, are not being studied extensively. A very limited studied have been done on the FCP for 2xxx aluminum alloys series.

As the size of specimen increases, the crack initiation also increases steadily along the length. From that, it can be concluded that in a large sized specimen, larger number of cracks would be develop as compared to the specimen of smaller size for a lower fatigue limit. The geometric factor is purely associated with the linear elastic fracture mechanics theory and is only be considered when the specimen has already a notch in it. A high level of non-linearity in the stress distribution may be observed when the structure has notches in it.

In Paris law, for the modeling of fatigue crack propagation, a very initial work in being done and this Paris model is still incapable to explain many crack propagation phenomena's i.e. stress

intensity factor, effect of stress ration and crack closure. Two types of new FCR models were being introduced by the researchers named, state space model and time scale model, and are dealing with the fluctuating amplitude loadings. Now the Paris model is being described as under:

$$\frac{da}{dN} = C(\Delta K)^m \qquad\qquad 1$$

Where $\frac{da}{dN}$ the FCGR, and "C" and "m" is are different testing parameters under testing and ΔK is the stress intensity factor[8].
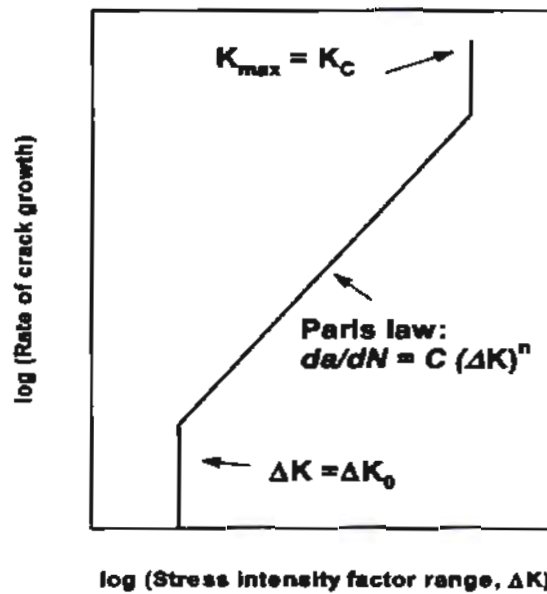
Fig. 1.2 Different regimes of Paris curve

Furthermore, Paris curve is being divided into three main regimes as shown. These are named as a) threshold regime b) power law regime c) rapid growth regime. Out of these three regions, the Power law regime in further divided into two sub regions which are not separated in most of the cases. That should also be kept in mind that the microstructure highly effects the fatigue crack propagation rate of that material.

The subzones of power law regime are named as intermittent zone and zone of continuous growth zone. The elastic modulus of fatigue crack growth is mostly associated with the second subzone. For the lower value of ΔK, the fatigue crack propagation is not growing with each and every cycle

but it grows occasionally in accordance with specified period and the distance between these two periods is calculated by the distance between the two adjacent striations[9].

For the high values of SIF, the fatigue crack growth rate varies by a factor of 20. This phenomenon mostly happens in the case of aluminum alloys AA22xx series. Whereas, for the lowers value of stress intensity factor, in Paris curve with a very less scattered data, this factor may drop to 4.5.
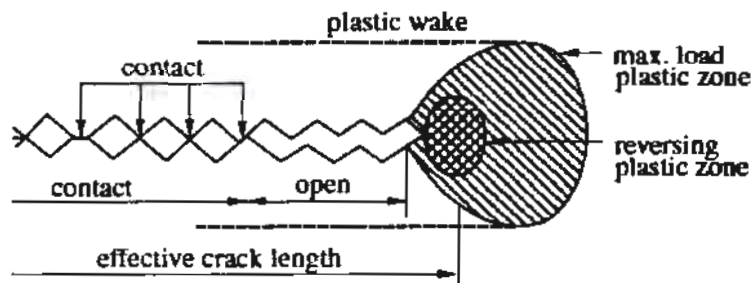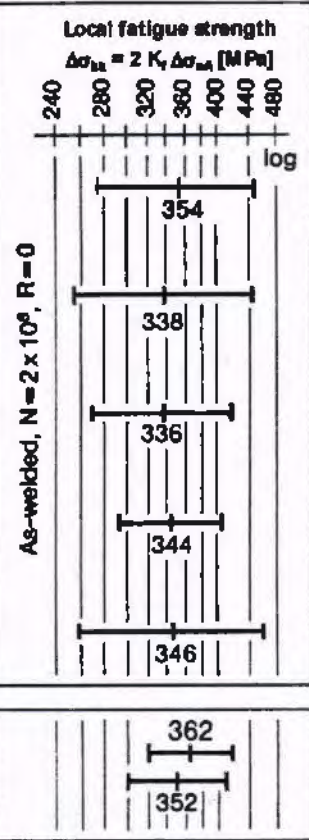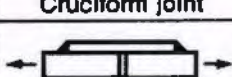
Fig. 1.3 Crack closure behavior

In the investigation of fatigue crack propagation, crack closure plays a vital role and has been found a very dominant factor by the researchers. Researchers have made a lot of efforts to find out its impact of means stresses in the FCGR based on the phenomenon of crack closure[10].

The crack closure, which is produced by the plasticity in the crack growth areas and except for the high values of ΔK and higher stress ratios, it affects the fatigue propagation in the Paris region. The load parameters of normalization can better explain the effects of means stresses on the fatigue crack growth rate hy using the crack closure technique. It can be observed from the previous literature and experimental results that the fatigue crack propagation in the Paris region is not mainly depending upon the microstructure of that material when dealing with K_{eff}, However, when the value of da/dn are taken against the ΔK, it showed that the microstructure of that material influenced the behavior in Paris region[11].

Mostly the alloy AA2219 is welded using TIG type and most frequent joint type is butt joint. It is considered that simply fatigue failure covers the most of disasters occurs due to fatigue failure of welded joints. Although the fatigue properties of aluminum are so nice but the problems are generated when there is sudden change in structure takes place.

Table I Different welding joints type and their characteristics [1]

Welded joint type (Structural steels)	Fatigue notch factor K_f	Nominal fatigue strength (R = 0) σ_{nA} [MPa], P_s =			Local fatigue strength $\Delta\sigma_{kA}$ = 2 K_f $\Delta\sigma_{nA}$ [MPa]
		10%	50%	90%	
Butt joint	2.27 Weld toe	61	78	99	354
Transverse stiffener	2.45 Weld toe	52	69	91	338
Cruciform joint	2.50 Weld toe	54	67	83	336
Overlap joint	3.12 Weld toe	47	55	65	344
Cruciform joint	4.03 Weld root	32	43	57	346
T + Y joints	Results for crane constructions	As-welded Stress relieved			362 / 352

During the TIG welding of aluminum plates it is visualize that a continuous bead structure is formed and these beads have a very drastic effect on fatigue life of specimen. It is also concluded that there is large effect of temperature produced during TIG welding along with the mixture of shielding gases on total fatigue life of the specimen. Normally for aluminum alloys, the fatigue life is increased when the testing is performed on low temperature while it is decreased when shielding is increased[12].

Effects of residual stresses and HAZ on crack propagation are studied for welded aluminum keeping the crack parallel to already mentioned zone and orthogonal in second case. The results show that crack propagation rate is slower and higher than parent metal depending on distance of crack from the weld center and crack orientation.

With respect to pre heating conditions and temperature during the period of interpass, the impact energy and fracture persistence of heat affected zone and weld nugget zone is very much less as compared to base metal, although the these regions have good weld ability[13].

It is already investigated that with respect to tensile strength and structural performance, the base metal is much better than the welded metals. The reason is that during the welding of metal there are considerable changes takes place in microstructure having very poor consistency like containing both the harder zones along with the very fragile ones.

All aluminum alloys are susceptible to high temperature cracking. The main problems monitored for welded aluminum structures are (a) cracking during the process of solidification of the molten pool (b) abundant fissuring at micro level in semi melted zone of heat affected zone of weldment[14].

A considerable enhancement in tensile strength and fatigue life is experienced by the welded metal when it is heat treated after welding and let it for aging for different time periods. For some heat, treatable aluminum alloys the mechanical properties of heat affected zone (HAZ) are degraded up to such level that it can only be improved when a complete heat treatment process including the aging is done.

AA2219 is a binary alloy (Al-Cu) along with the small quantities of Mn, Ti, V and Zr. It is heat treatable aluminum alloy which changes the phases after precipitation. The term wise precipitation arrangement is as (i) α-Al (ii) secondary particles along with the GP zone. It exists either in the form of solid solution or in the form of metastable and stable phases[15].

Extensive use of AA2219 after a reliable heat treatment in aerospace industry needs a fail-safe material behavior prediction. After welding the distribution of second phase particles in solid solution of aluminum alloy affects the mechanical properties of whole structure. Most of cryogenic tanks are fabricated by using AA2219 sheets that are pre-heat treated. The most reputable welding types used for this aluminum alloy is TIG welding[2].

Thermal cycles produced during the TIG welding process are main cause of microstructural evolution in AA2219 leading to variations in mechanical and structural properties of subjected
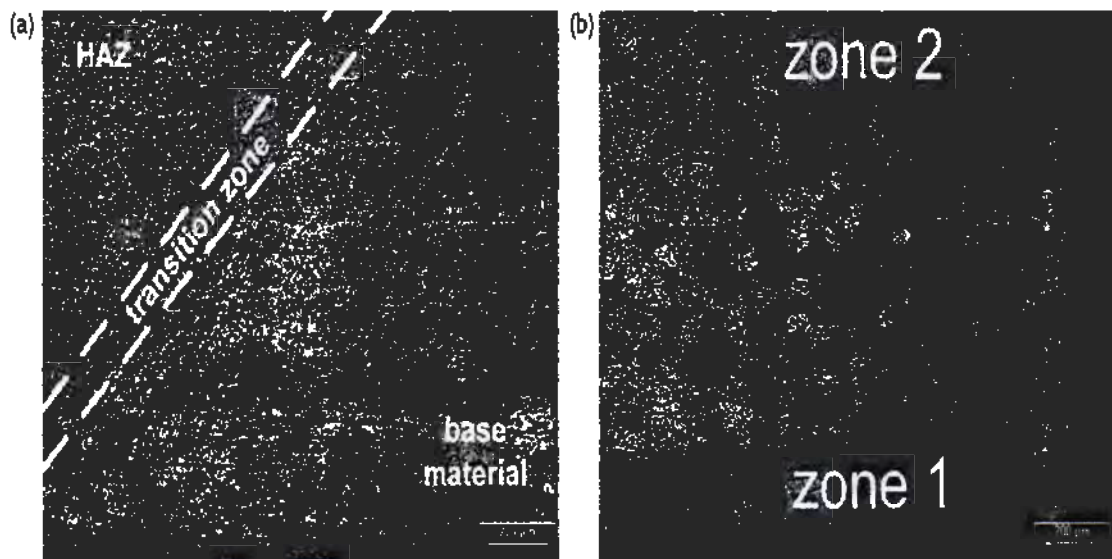
Fig. 1.4 Different microstructural zones formed after welding [2]

material. However, fatigue properties are totally controlled by the top surface microstructure rather than the cross sectional.

The effects of specimen's thickness on mechanical properties are well known. It is investigated that as the thickness of welding toe is increasing the fatigue strength decreases. Recently the researchers have revealed that the specimen thickness influences the fatigue strength and other properties of weldment. 25 mm is the standard thickness which is usually taken [16].

For a failsafe design, many thickness correction factors have been introduced. It is normally represented by "p" and as per international recommendation, it ranges in value from 0.3 to the value of 0.1. From the results, it is also observed that the correction factor also depends upon the topmost value of stress intensity factor. However, thickness correction factor can only be used for the specimens which are not adjacent to reference thickness[17].

Welding joints also play a vital role in the fatigue strength of that material. Every joint has its own behavior for fatigue strength like longitudinal butt joint, transverse butt joint, fillet joints and transverse cruciform joint have diverse manners for the fatigue strength[18].

Welding speed along with the welding pass during the TIG welding process also has different effects on fatigue crack growth. It is visualized that aluminum alloys welded at high speed have a small heat affect zone and in other words baving less fragile zone. Multipass TIG weldment have

low fatigue strength as compared to single pass as the coarseness of second phase particles increases in solid solution of aluminum alloy when applied a second pass. It is also examined that the cover area of heat affected zone also increases during the multi-pass TIG weldment[19].

Existing defects along with the manufacturing defects have smart effects on fatigue strength of aluminum alloys. Different types of flaws and porosities assist in fatigue crack propagation. The shear forces on the boundaries of flaws made them in such a way that they themselves behave as a crack.

Different grain refinement techniques define the inter-granular or Trans granular fatigue crack propagation. Grain boundaries concentrations also affect the fatigue crack speed. Grain boundaries with different concentration of secondary particles in aluminum alloys have different fatigue strength.

The concept of nominal stress is still predominant in many technical fields. The definition, value of nominal stress and its allowable value conforming to that structural stresses are necessary to find out for its application. The fatigue design categories of the welding structure are truncated by the fatigue design class (FAT) and a corresponding number is combined with it. They represent the design code of that specific welding joint[20].

Curve for fatigue designs holds true for any value of R ratio. However, we only apply the load concepts when dealing with the more complex structures because both nominal and structural stresses fails to deal with that structures. Fatigue design curves are valid for any R ratio. The application of local concepts can be justified in the way that fatigue growth has a local phenomenon and this cannot be defined by the nominal stresses. The local concept being used can be further classified into three major categories. Notch strain or strain concept, elastic structure strain or structural concept and fracture mechanics concept. Every group is further divided into subgroups which are shown in Figure 1.6. Both seems spot welded joints are written side by side on both sides[21].

It is not the aim of following contribution to give a status report on local concepts which can be derived from the authors recently republished and actualized standard work and its prior reviewing publication. It is aimed to review some more recently proposed special variants of the local concepts which are under controversial discussion at the time being. The presented concept

variants and related issues are arbitrary to some extent, but the authors hope that the selected concept variants will be of lasting value. Before giving the details about the selected fatigue assessment methods, the basic physical facts behind these methods are recapitulated. The fatigue life in numbers of load cycles consists of the technical crack initiation life and the subsequent long-crack propagation life up to final fracture. The technical crack may be a surface crack, about 1 mm in depth and 2 mm in length. The technical crack initiation life comprises the microstructural crack initiation life and the short-crack propagation life up to the technical crack size. In un-notched specimens, most of the total life may be consumed in microstructural crack initiation. In sharply notched specimens, on the other hand, the crack initiation life may be very short, but initiated cracks are arrested to some extent. These basic physical facts are not mirrored in the conventional global and more recent local fatigue assessment methods for welded joints except for technical crack initiation and long-crack propagation in some cases[18].

1.4.1 Contributions to the Structural Stress Concepts

The term 'structural stress' designates the basic stress in a structure in areas of geometrical inhomogeneity, where fatigue cracks are initiated ('hot spots') while the notch effect is ignored. Engineering methods of structural analysis, the finite element method among them, ignore the notch effect in general so that structural stresses are determined. Another, less convincing elder name for 'structural stress' is 'geometric stress'. The original idea of the structural stress concept has been proposed in terms of structural strains. The local strain in front of the weld toe measured by a strain gauge serves as the parameter for
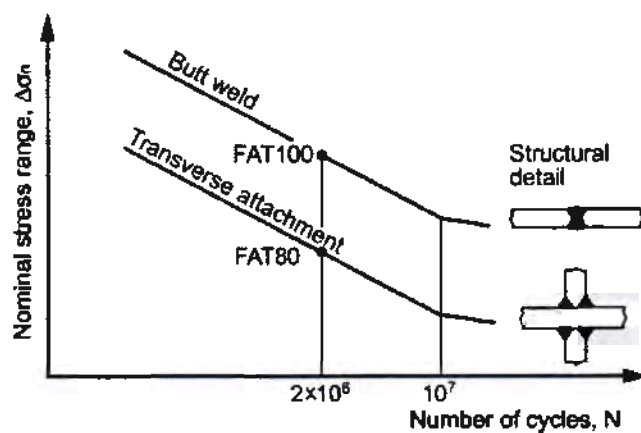
Fig. 1.5 S–N curves in the nominal stress concept[18]

Local concepts	Structural stress or strain concepts	
	Structural strain	Structural stress
	Notch stress or strain concepts	
	Elastic notch stress	Elastic-plastic notch strain
	Fracture mechanics concepts	
	Crack initiation	Crack propagation
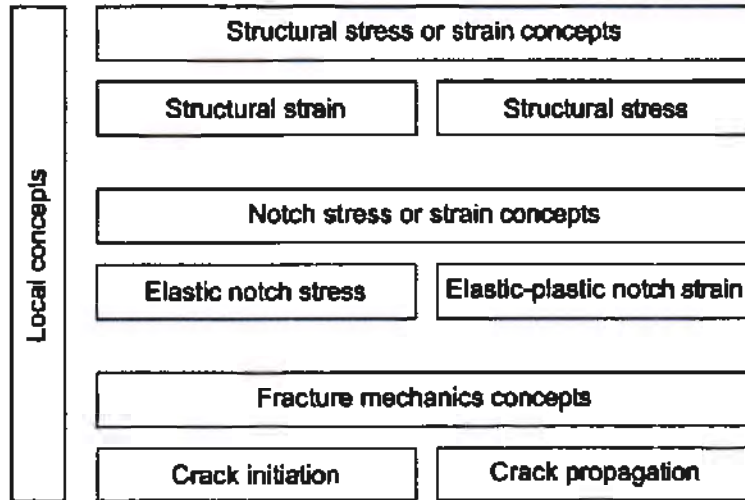
Fig. 1.6 Classification of local concepts of fatigue assessment of welded joints.

fatigue assessment[22].

With the introduction of the finite element method, the structural stress variant which was developed for tubular connections in steel constructions (roofs, bridges, off-shore structures) gained in importance and led to the hot spot structural stress concept as a codified procedure of fatigue assessment. In this method, the surface stresses at prescribed evaluation points in front of the weld seam are linearly extrapolated to the weld toe. Later, the concept was transferred from tubular connections to plate and shell structures of ships and other technical equipment.[23]

The structural stresses depend, besides on the type and level of loading, on the shape, dimensions and arrangement of the components in the welded joint. In the method above, predominantly the normal stresses perpendicular to the weld seam affect the strength. Thus, the structural stress concept first of all serves for the evaluation of strength under loading in this direction.[24]

1.4.2 Conventional Structural Stress Concept

In general, welded tubular joints are distinguished from welded non-tubular joints. The latter joints are considered in the following, that is, the structural stress concept is applied to plate-type structures. The conventional method of determining the hot spot structural stress is the linear or nonlinear extrapolation of measured surface stresses to the weld toe (two or three evaluation points at locations. The extrapolation of surface stresses is also applicable hased on finite element models. For shell or plate structures the internal linearization of the cross-sectional stresses gained from

11

structural analysis offers an alternative. Systematic investigations revealed the need of detailed rules for finite element modeling and stress analysis in order to avoid too large scatter and uncertainties of the results. A special problem is structural distortions caused by the fabrication process, especially axial and angular misalignments. Because the structural stress design S–N curves are based on measured structural stresses, they already include the effect of specimen misalignment[25].
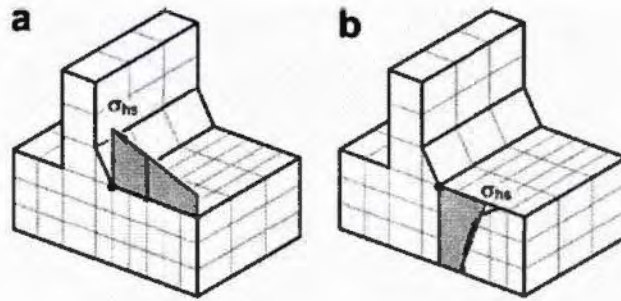
Fig. 1.7 Linear extrapolation of surface stresses[19]

Therefore, their application requires explicit consideration of the influence of misalignment on the actual structural stresses whereas within the nominal stress concept, this effect is implicitly considered to a certain degree in the nominal stress design S–N curves. In the normal case, the finite element models of ideal geometry, delivering the stresses, do not contain misalignment. In plate-type structures, the effect of misalignment on the structural stresses must be considered predominantly in butt-welded joints and in fillet-welded cruciform joints (because of a possible axial misalignment) as well as in fillet-welded one-sided transverse attachments (because of a possible angular misalignment). If no detailed data are available, recommendations suggest multiplication of the axial stress at the weld toe with given factors which consider the effect of misalignment in the range up to 15% of the plate thickness[26].

1.4.3 Contributions to the Notch Stress or Strain Concepts

Notch stress or strain concepts (also termed 'local stress or strain concepts') use the maximum elastic notch stresses or elastic–plastic notch strains, respectively, to assess the fatigue strength, (restricted to stresses). These stresses or strains can be calculated for the sharp or mild notches at the weld toe, weld root or nugget edge where the structural stresses have already been defined. One distinguishes between elastic notch stress concepts and elastic–plastic notch strain concepts. The elastic notch stress concepts were originally restricted to the high-cycle fatigue range. The

12

Elastic–plastic notch strain concepts apply to the medium-cycle and low-cycle fatigue range. The (elastic) notch stress concept for welded joints is based on the early work (notch support effect according to: critical distance approach). The elastic notch stress concept has been successfully applied to welded joints in steels and in aluminum alloys[27].
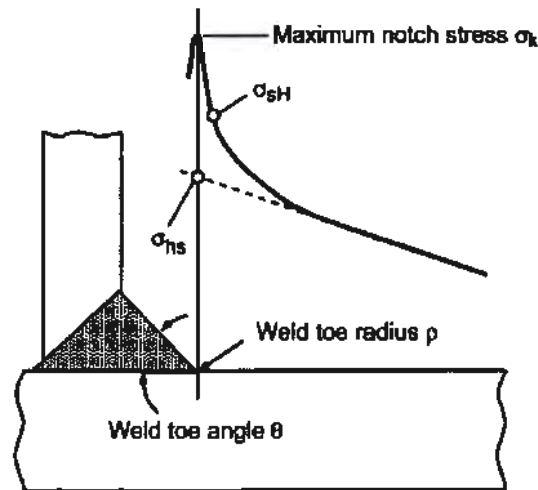
Fig. 1.8 Maximum notch stress σ in comparison to the hot spot

The (elastic–plastic) notch strain concept for welded joints (also early proposed by scientist, is based on developments for non-welded components loaded predominantly in the low-cycle fatigue range, incorporating Neuber's simple equation ('Neuber's rule') which relates the elastic–plastic notch strain to the notch stress in case of local yielding at the notch[28, 29].

1.4.4 Effect of Natural Aging on Al- Alloys

The effect of heat treatment and aging is that it changes the nuclei into the fine precipitates which changes the AA2219 mechanical properties because the size of precipitates and the structural distribution of nuclei controls the mechanical properties of Al alloys. Both properties have a serious impact on the results. After the heat treatment and aging, the morphology of the precipitates also changes and due to that, the results are far much different from the pre heat treated and unaged specimens [30, 31].

The effect of Natural aging, when the specimen is being kept at room temperature, limits the growth and applications of Al Alloys. The changes that takes place during natural aging limits its use. Accordingly, the problems that are being developed due to natural aging had been the area of

research of many scientists[32].They have investigated that the effect of natural aging on the yield strength of Al-Alloys. After extensive studies on that natural aging effect, they have concluded that the main effect of natural aging on the mechanical properties of Al–Mg–Si–Cu alloy (AA6111) was dependent upon the connections between the precipitates and the motion with which they dislocate after the natural aging. They have investigated that the response of Al–Mg–Si–Cu in regard of its hardness, the alloy in its T6 condition, its value decreases very sharply when keeping it up to 3h preceding to the room temperature. They have also investigated that it was due to the fact that by keeping the alloy for a longer time reversed the formation of main strengthening phase which is phase β [33].

Many researchers have also examined the natural aging effect on the hardening behavior of Aluminum alloys Al-Mg-Si by introducing aging in different and multi stages. After The results indicated that clusters/GP zones forming during natural aging could reduce the rate of hardening during subsequent multistage aging and the influence was more distinct during over-aging.[34].

2 *Experimental Setup*

2.1 Material

In this thesis, Aluminum alloy AA2219 has been used to study the fatigue crack propagation behavior in natural aged TIG welded and non-welded specimen with T-87 pre-weld heat treatment. It is a wrought aluminum alloy with copper as a main constituent. Due to its vast applications in aerospace and automobile industry, it is necessary to study its behavior on experimental basis. As cyclic or fatigue loading is the contrary factor for automotive and aerospace structures failure, it is highly recommended to test the material for fatigue crack propagation.

Table II Chemical composition of AA2219

Alloy	Al	Si	V	Cu	Mn	Mg	Zr	Ti	Fe	Zn
AA2219	Balance	0.2	0.04	6.3	0.3	0.02	0.18	0.06	0.23	0.04

The chemical composition of aluminum alloy is shown in above table which portrays that the main ruling alloying element in AA2219 is Cu.

Due to its high strength to wait ratio, it is highly suitable for the manufacturing of cryogenic tanks. The profusion of Cu in AA2219 and other alloy of 2XXX makes it highly suitable for the aerospace industry. The solidus and liquids temperature of AA2219 are noted to be 543°C and 643 °C respectively. The annealing temperature of research material is nearly 413°C.

Mechanical properties of AA2219 are listed below in Table II.

Table III Mechanical Properties of AA2219

Hardness, Vickers	149
Modulus of Elasticity	73.1 GPa
Tensile Strength	170 MPa
Poison Ratio	0.33
Shear Modulus	27 GPa

The ultimate tensile strength of subjected AA2219 material can be improve by applying different heat treatment techniques. There are two methods that can be used to enhance the strength of AA2219 which are:

- Solution Heat Treatment
- Precipitation Hardening

The most common one between these two is the solution heat treatment process.

2.2 Pre-Weld Heat Treatment (T87)

The subjected aluminum alloy AA2219 is increased by employing pre-weld heat treatment process instead of post-weld heat treatment process which is being investigated by different researchers in the past. According to ASTM international, for best aerospace properties, the suitable pre-weld process is T-87. The detail preview of this type of pre-weld heat treatment has been shown in Figure 2.1.
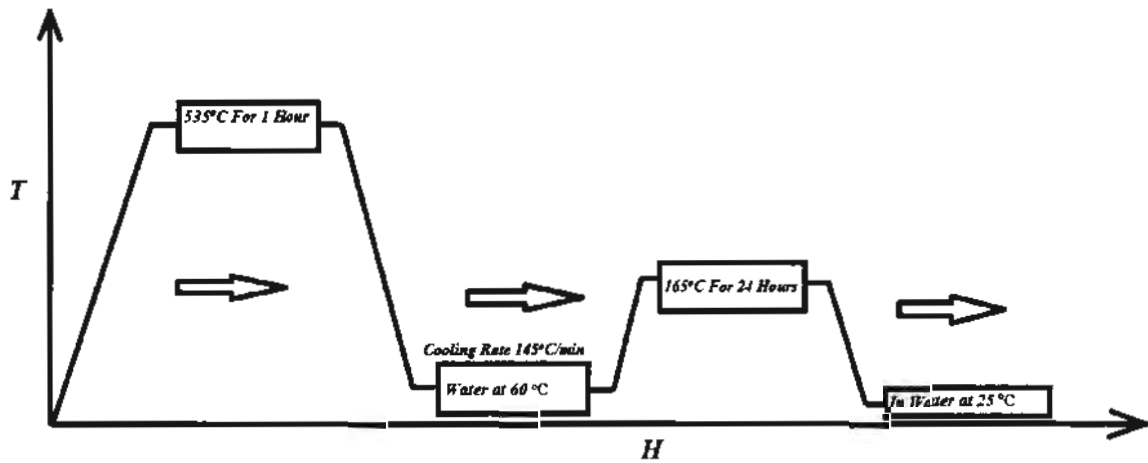
Fig. 2.1 Details of T87 Heat Treatment

A digital and sophisticated electric furnace is being used for that heat treatment process. Initially the plates were kept in the furnace and temperature went on increasing. The set temperature was 535°C and the calculations were being done till the temperature reaches.
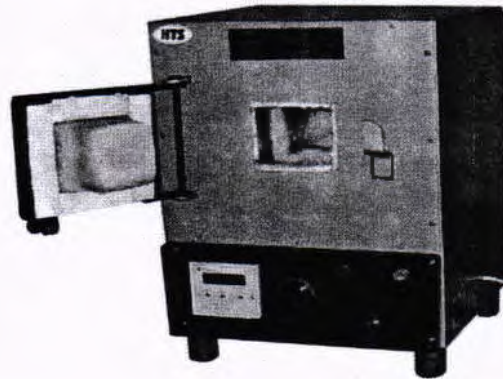
Fig. 2.2 Digital Portable Electric Furnace used for Pre-heat treatment [2]
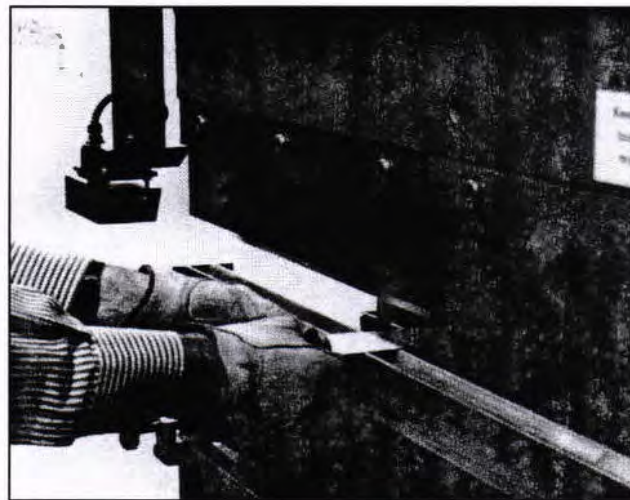
Fig. 2.3 Aluminum sheets cutting under press cutter machine

2.3 Specimen Preparation

2.3.1 Non-Welded Specimens

The pre-heat-treated aluminum plates from the electric furnace are being cut with the help of hydraulic press cutter machine. One thing should always be kept in mind that the aluminum plates should be placed on a smooth surface and clamped tightly against the cutter blade so that the chance of edges beveling can be eradicated.

The specimen are than cut according the measurement of CT specimen with the help of press cutting machine and loaded on the horizontal milling machine for surface finishing. The slots in the specimen are also fabricated using the slotted cutter.

Fig. 2.4 Horizontal milling machine

The compact tension specimen diagram as per ASTAM E399 has been shown in Figure 2.5. The specimens for this research work are made according to that particular standard with allowable tolerances.

2.3.2 Welded Specimens

In the preparation of welded specimen, the pre-heat-treated aluminum specimens are again cut into two pieces by press cutter machine lengthwise.

The matching corners of two different pieces are being tapered by using sbaper machine. All four corners should be tapered in such a way to make a "V" grove. By doing this, the matching sides of two pieces come in front of each other and a uniform filling of filler material is possible during
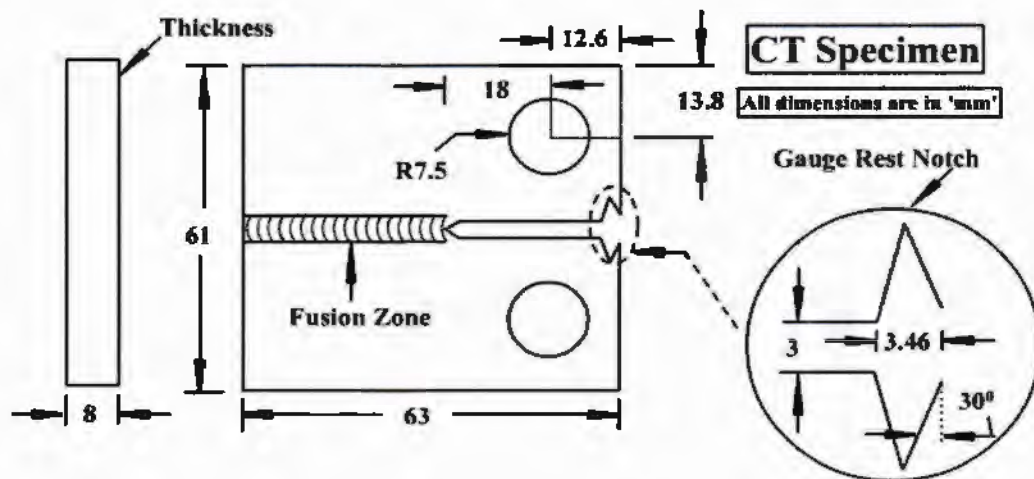
Fig. 2.5 CT Specimen

the TIG welding process. In other words, we are getting a strengthen butt joint and the true properties of weldment.

2.4 TIG Welding

The next step is the Tungsten Inert Gas Welding, in which two different types of electrodes and an inert gas is being used. The one electrode is non-consumable and is made of tungsten while the other consumable one is made of filler material which is compatible with the subjected alloy. In our research work, the filler electrode is AA2319 which is highly recommended by the researchers. Due to high melting point and good electric conductivity, tungsten electrode safe from being burning up.
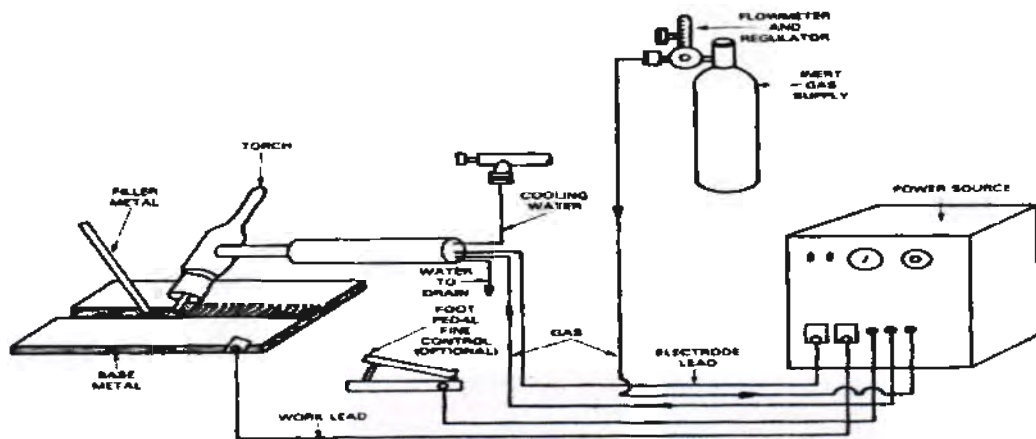
Fig. 2.6 A process schematic of TIG Welding process

Following three are the pre-requisite for TIG welding:

(i)   Filler alloy

(ii)   Shielding

(iii)   High Temperature

During the welding process, heat is generated when the electricity passes from non-consumable tungsten electrode. To cope with this heat, shielding is required which is provided by cylinder compressed with inert gas (protects the flame from air or in other words, protects the weldment from unnecessary oxide formation).

The other consumable electrode is AA2319 which is in the form of wire and placed in the welding zone with hands. The filler alloy melts and fills the groove. The gas valve is provided with the torch and controlled from it. The welded provides shielding effect many times during the whole welding process to avoid any misfortune.
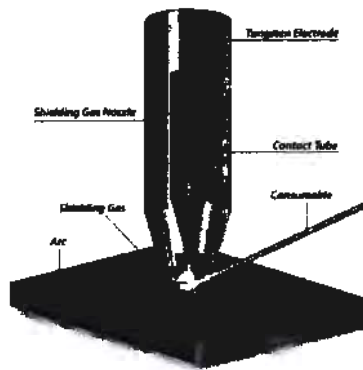
Fig. 2.7 Shielding Effect during TIG Welding

As soon as the arc create, it starts to melt the metal plate and produces a pool. Once this puddle is being created, the consumable electrode starts to melt the filler alloy and produces the weldment.

For aluminum TIG welding, a few points should be considered:

(i)   Non-consumable electrode should be of pure tungsten or zirconium tungsten.

(ii)   The current used should be A/C type.

(iii)   Puddle should be shiny for a perfect TIG welding of aluminum.

(iv)   Non-consumable should have ball shaped end so that heat distribution should be uniform and properly.

(v)   Overheating of metal should be avoided.

(vi)   welding starting frequency should be high.

In this research, the filler alloy used for the welding of AA2219-T87 is AA2319 which is highly suitable and compatible for this alloy. The chemical composition of AA2319 is shown in Table III.

Table III. Chemical composition of AA2319 filler alloy

Alloy	Al	Si	V	Cu	Mn	Mg	Zr	Ti	Fe	Zn
AA2319	Balance	0.2	0.02	6.3	0.3	0.02	-	0.015	0.3	0.18

The TIG welding machine MW2600-380 is being used for the welding having current varying capacity of 3A to 300A. During welding process, it has demanded that the Ar purity should be kept constant at 99.9%. Square–butt joints are produced by using fillers of AA2319 by varying the voltage of 35V and current of 200A. Initially speed of welding is kept slow after some time, it was maintained at 4-5 ipm for voids and porosity free weldment. Initially the flow rate of inert gas was kept at 14 L/min and then maintained at 16-18 L/min during the weldment.

2.5 Natural Aging

After the plates are being cut and transformed into the standard specimens, they were kept for natural aging on room temperature. They were placed for a period of 03 months which is a standard procedure for natural aging. After the natural aging, the specimens were ready for the microstructure evaluation and fatigue testing as per the ASTM E399.

Fig. 2.8 AA2219 Aged Specimen

2.6 Micro Hardness Test

To check the hardness of Aged AA2219-T87 specimen, Brinnell hardness test was performed on the HBRVU-187.5, a Brinnell, Rockwell & Vickers hardness testing machine available in fracture mechanics and fatigue lab, UET Taxila.
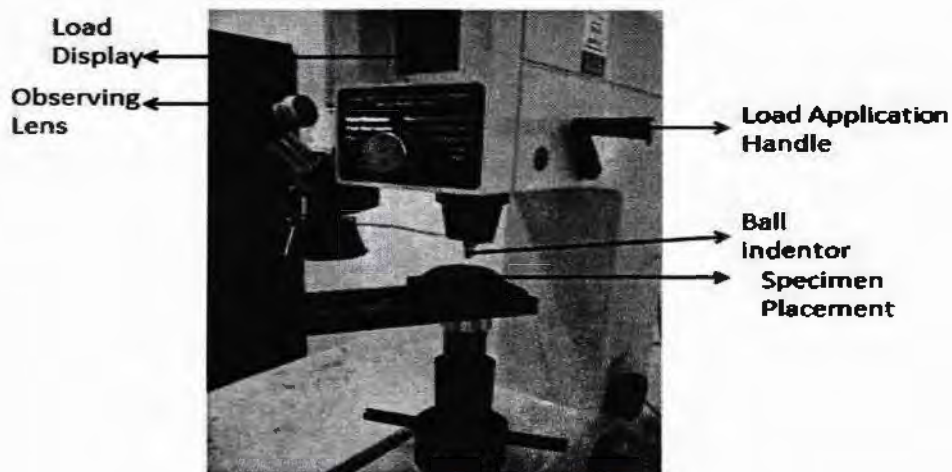
Fig. 2.9 Hardness Tester

The history of Brinnell hardness test was started during the World War II to find out the hardness of the plates used in war. In this test, a steel or carbide indenter is pushed into the metal under a specified loading. Because of this force, an indention is left behind in the metal specimen which is then measured and Brinell hardness value is calculated from the formula. The smaller the indention, harder the material is.

Fig. 2.10 2.5 mm Steel ball indenter

Hardness test is another form of tensile test. Besides the base metal, the hardness value of welded specimen is also required because due to the high temperature of welding, different welding zones are formed and the mechanical properties are altered due to that abrupt changes. So, it is necessary to find the hardness value from the center of weld tip of specimen so that the welding effects can be studied on the subjected material and the filler alloy.

Detail description of hardness test is as under:

2.6.1 Procedure

Diameter of the steel indenter used is 2.5 mm and the applied load is 613 newton (62.55 kgf). They are selected from the information provided by the manufacturer of the tester. The Brinnell hardness value of the specimens is obtained to be 101.38 BHN. The formula used to calculate the value of Brinnell hardness value is given in Eq. 2

$$BH = \frac{2F}{\pi D \left[D - \sqrt{(D^2 - Dl^2)}\right]}$$

2

Where:

BHN = Brinnell hardness number

F = Applied load in kg

D = Diameter of the spherical indenter in mm

Di = Diameter of the resulting indenter impression in mm.

The indentation is circular so the vertical and horizontal readings are taken by measuring the diagonal values d1 and d2
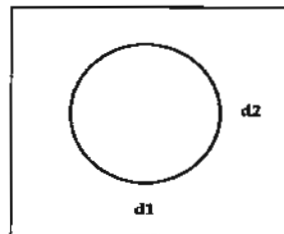
Fig. 2.11 Horizontal and vertical diameter

0.004 is the least count of the tester. In Table IV, which is the method of calculating the hardness number, represents the supposed value. From the values of the BHN obtained above, an average

Table IV Brinnell Hardness number calculation for AA2219

Sr. #	Horizontal Reading d_1	Vertical Reading d_2	$D_i = ((d_1 + d_2)/2)$ *0.004	BHN $= 2F/\pi D(D - \sqrt{(D2 - Di2)})$
1	215	206	0.842	109.11
2	213	308	1.042	70.04
3	213	205.5	0.837	110.5

value has been calculated. The mean value comes out to be 96.55. Tbus, the Brinnell hardness number of the Aluminum specimens is 96.55 BHN.

2.7 Fatigue Test

To examine the fatigue crack propagation behavior of the subjected material, a servo hydraulic universal testing machine (MTS 810) has been used in this research work which shown in Figure 2.11. This machine is available in fracture mechanics and fatigue laboratory of UET Taxila. All fatigue tests are being carried out at a stress intensity ratio of R = 0.1. Initially, the frequency was kept 20 cycles/sec. That was for the initiation of crack in the specimen. It was then reduced to 5 cycles/sec and later on 02 cycles/sec when the crack propagates rapidly so as to avoid fracture of specimen.

Fig. 2.12 Universal testing machine model MTS 810

2.7.1 COD Gauge Data

MTS 810 is supported with a complete data acquisition system and an auto file is generated in the connected computer having a range of crack displacement against the respective cycles. In other words, a complete file of complete test is being generated with the auto build system of MTS. A complete waveform of test is also formed and can easily be obtained from the data acquisition system.
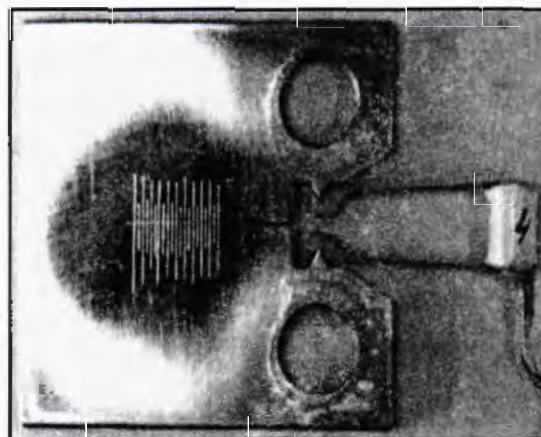
Fig. 2.13 0.2 mm graduated CT specimen

2.7.2 Optical Data

Besides the data produced by the MTS, it is necessary to modify the machine and take data from that means as well to compare on later stages. For such modification, two methods are commonly employed with universal testing machine by the researchers which are briefly describe as under:

2.7.2.1 Manual measuring of crack length

In this type of modification, a light microscope is attached to the column of the fatigue testing machine to check the crack length with a single eye piece on it. The front section of the microscope is kept near the specimen under cyclic loading. The studying area of the loaded specimen is graduated with small equidistant lines i.e. 0.2 mm with the help of electric discharge machine (EDM).

As soon as the crack starts, the graduated lines are calculated from the starting point of the crack till the end of crack tip from the eye piece of attached microscope and repeat the cycle after different intervals. This procedure is repeated on fixed intervals and a data chart is obtained.

Due to some technical difficulties and reading problems, this method has been restricted to only single fatigue test. This was only used when computer controlled digital microscope was not available in fracture mechanics & fatigue lab.

2.7.2.2 Vernier caliper measuring crack length

Now a day, a modern and sophisticated attachment is available with MTS. In this technique, a light microscope attached with a computer or laptop is fixed in front of specimen and the display of which can easily be viewed on the screen.

The microscope is attached in such a way that its foundation is fixed at the top edge, the crack initial point is marked with removable marker. When the crack starts propagating, the microscope is advance further and the crack length is calculated using the Vernier caliper.

In comparison of the other one, this technique is more reliable and is widely used in the fatigue testing. By using this technique, exact values of crack lengths can be obtained and when the crack length crosses a certain limit, there will be no complexities in data acquisition.

3 *Microstructure Evolution*

3.1 Introduction

Aluminum and its alloys have assorted applications in automobile and aerospace industry which depicts the importance of right selection of welding technique for respective method. Due to the inducing of residual stresses and the structural change, the welding of aluminum and its alloys is always remaining a tough and chore challenge for the designers. Different alloys of the said material which belongs to the family of 2XXX, 6XXX and 7XXX are mostly used in the above mentioned industries because of their high strength to weight ratio, good weldability, good formability and high resistance to corrosion[35].
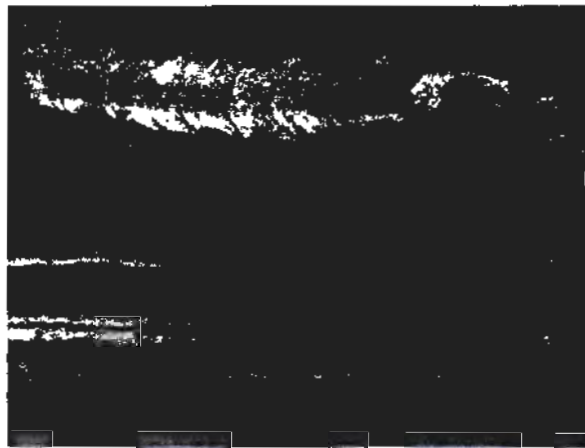
Fig. 3.1 Failure of TIG weldment in aluminum alloy

There are numerous factors allied with the welding process as the augmentation of thermal conductivity and expansion coefficient, manifestation of tenacious oxide coating, solidification shrinkage and the most overwhelming one is the trapping of gases during the molten state.

The behavior of welded and heat treated aluminum alloys remains a key subject of investigation of researchers for decades because the heat evolved during the welding abruptly changes the mechanical properties due to the phase shifting of alloys. Due to welding, a weak zone is formed near the welding zone which is responsible for strength decline of that zone. It is highly considered that the precipitation of molten alloys, the recrystallization and nucleation of grains developments are the key factor for the softening of this zone. Grain development are liable for softening of this zone.
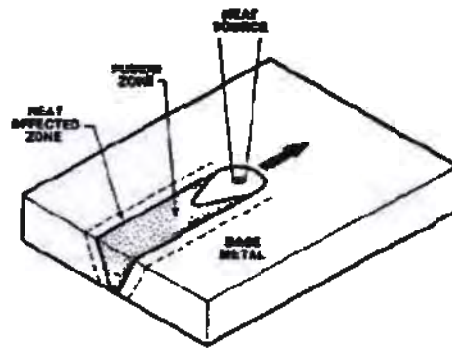
Fig. 3.2 Schematics of different zones generated after welding

Extensive research has been made to reinforce this zone by applying different welding techniques, post and pre-heat treatment processes and the erraticism in these methods. From the microstructure evaluation, different zones are formed after the welding process with all have different characteristics.

3.2 Apparatus for Microstructure Examination

To study the microstructure of given AA2219, two type of apparatuses are available in UET Taxila lab named as Metallurgical Microscope (Olympus D-20) and the other is Scanning Electron Microscope (SEM). A brief description of both apparatuses is given as under:

3.2.1 Metallurgical Microscope

As the subjected metallurgical microscope is equipped with five different lenses having different magnifications, the microscopic study is more instructive. For suitable metallographic view, a range of image light appearance is also available in Olympus DP-20.

A comprehensive data acquisition system is also available which supports the automatic storage of captured metallographic pictures.

Fig. 3.3 Metallurgical microscope (Olympus DP-20)

3.2.2 Scanning Electron Microscope

The other sophisticated and latest technology used for the finer and reliable grain structure is SEM. Now a day, researchers mostly rely on SEM and TEM analysis. By using this apparatus, fine grain structures with fine details have been studied.
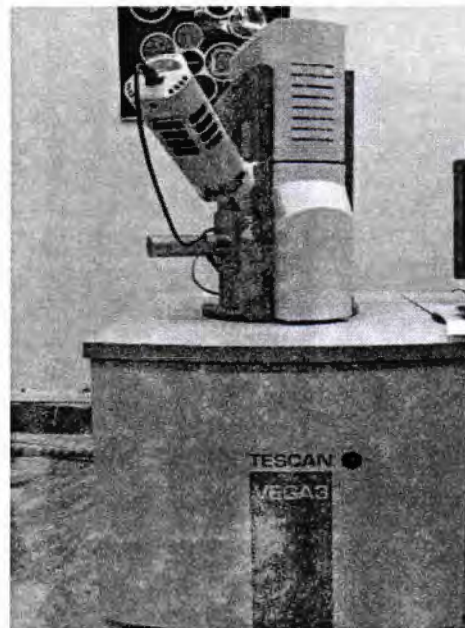
Fig. 3.4 Scanning Electron Microscope

29

3.3 Specimen Preparation

3.3.1 Surface Preparation

For metallographic study, it is necessary to prepare the specimen as per ASTM E399 which is a specific process because due to the aging and keeping the specimens for a longer period produces a layer of oxide on the upper surface which make it difficult to observe the grain structure.
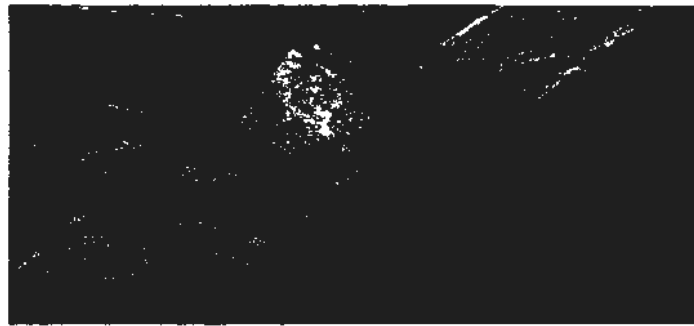
Fig. 3.5 Emery papers of different grades

After the etching has been done, for nonferrous metals especially in the case of aluminum alloy, a fine oxide layer is being formed. Another difficulty which is being faced during the surface preparation is that even a minor over etching because the grain structure to disappear.

Due to all the above troubles, a great care has been done during the surface preparation because a little negligence in etching can lead to the wastage of specimen.

A detail method of specimen preparation is given below

> First step is to remove the scratches and abrasion from the specimen surface. For this purpose, the emery papers of different grades are being used. Aluminum and other soft metals need sandpapers of high grade. When the specimen felt soft and scratch free, then the emery paper was changed with relatively greater number and reached the maximum higher grade i.e. 2000.keep it in mind that the emery papers works best with kerosene oil.

> After the specimen surface preparation with emery paper, the surface still needs some more finishing and this is done with the help of buffing. The buffing is done with thick fibers and then with thin fibers.

➤ During buffing the specimen attains higher temperature because of the friction phenomenon. To avoid any mishap, leather gloves should be used and the specimen were dipped regularly in cold water after short interval of time. It is also important to keep the specimen free from the thermal stresses to obtain a better and clear grain geometries.

➤ After the buffing, the next step is the application of polishing paste and creaming it. This process was performed to polish the specimen and to remove the entrapped dust or other particles to make the surface more shiner and clean.

➤ The next and final stage in the specimen surface preparation is the application of diamond paste of different sized. After the application of polishing paste, the specimen is washed with a bulk of fresh water and diamond crystal paste is applied.

Fig. 3.6 Rough and fine diamond crystal paste

There were three different sized diamond paste available in FMF lab UET Taxila. Everything were applied from rough to finer size. Diamond crystal paste is very helpful in visualizing the grain geometries.

3.3.2 Chemical Etching

All the above discussed postulates of specimen preparation are mechanical in nature. After applying all these processes, the specimens are finally prepared by the chemical treatment which is referred to as the chemical etching. The chemical etching requires a much experience hecause requires very calculated time, especially for soft metals.

According to ASM standards, the chemical etchant for AA2219 is Keller's Reagent[36]. The concentration of different chemicals is listed helow:

> 5ml HNO3 (conc.)
> 2ml HF (48% conc.)
> 3ml HCL (conc.)
> 90ml distilled Water (H_2O)

When etching has performed properly, a clear and fine grain structure can be obtained. One thing should always be kept in mind that best results of microstructure observation can be done only by freshly etched specimen. A greater care should be done during the etching process and specimens should be dipped in solution with the help of Plier or any other tool.

After completing the etching process, wash the specimen with fresh water for a considerable time before placing it on the metallurgical microscope.

3.4 Microstructure Evaluation (Before Aging)

From previous literature, it is observed that the mechanical properties of solution type alloys are significantly affected by primary grain structure. Particularly the alloy which is being used in this research, a clear and uniform micro grain structure is necessary to check the anticipated mechanical properties.

3.4.1 Base Metal (BM)

Before the welding, AA2219 is a solution type solid in which the main constituent Cu atoms remains dissolve in the lattice structure of α-Al to form the monophasic structure which is clear from the Figure 3.7 of aluminum-copper phase diagram.
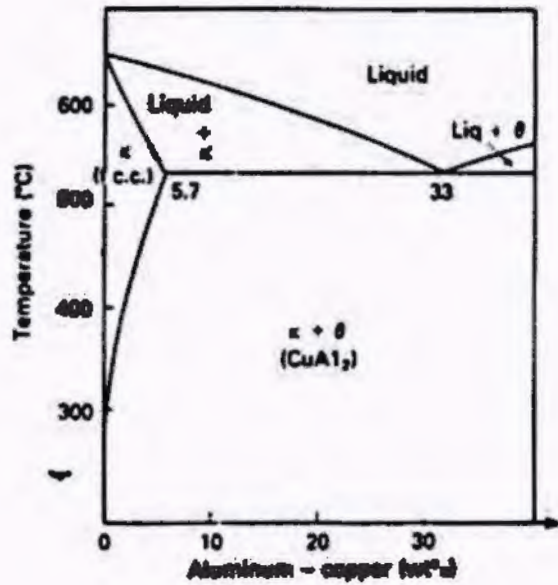
Fig. 3.7 Al-Cu phase diagram[31]

Because of the effect of heat treatment (T-87) of AA2219 base metal, the intermetallic structure of Al$_2$Cu, which is 53.1 % by weight and having an irregular geometry, are already present in the micro grain structure as shown in Fig. 3.8 the grain is rolled and extended.

The presence of second phase particles (Al$_2$Cu) can also be seen within the grains and along the grain boundaries[37]. The precipitate free zone (PFZ), which rarely appears in the structure, can also be seen in this Figure 3.8.
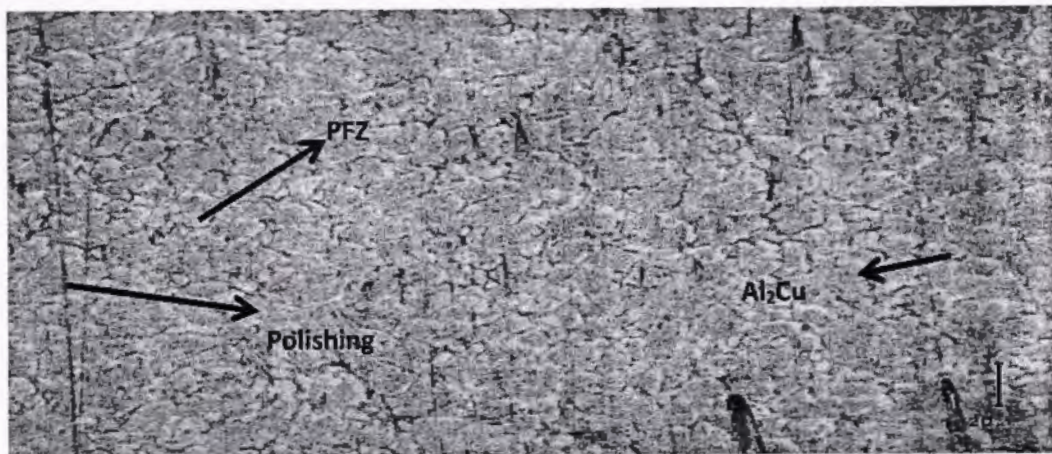
Fig. 3.8 Grain structure of base metal (AA2219-T87)

The intermetallic can clearly be viewed in the micro grain structure which supports the fact that some sort of aging is already been done on the base metal before welding is being performed. Due to that aging, precipitate hardening has been done on the surface of base metal whereas grain boundaries defects can clearly be seen in the picture above.
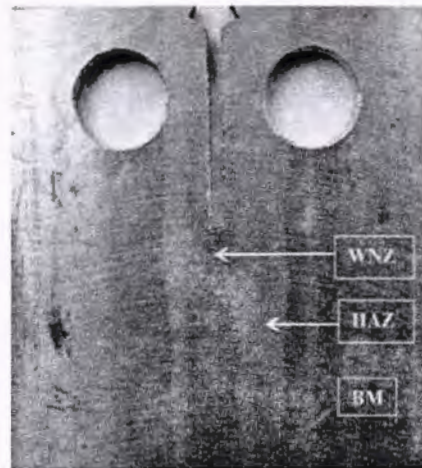
Fig. 3.9 Different regions of welded AA2219

3.4.2 Heat Affected Zone (HAZ)

The zone between the BM and WNZ is the heat affected zone (HAZ). Due to the higher temperature of welding process, the mechanical changes take place abruptly in this zone but the molten pool of weld metal is not formed as that appears in the case of weld nugget zone.
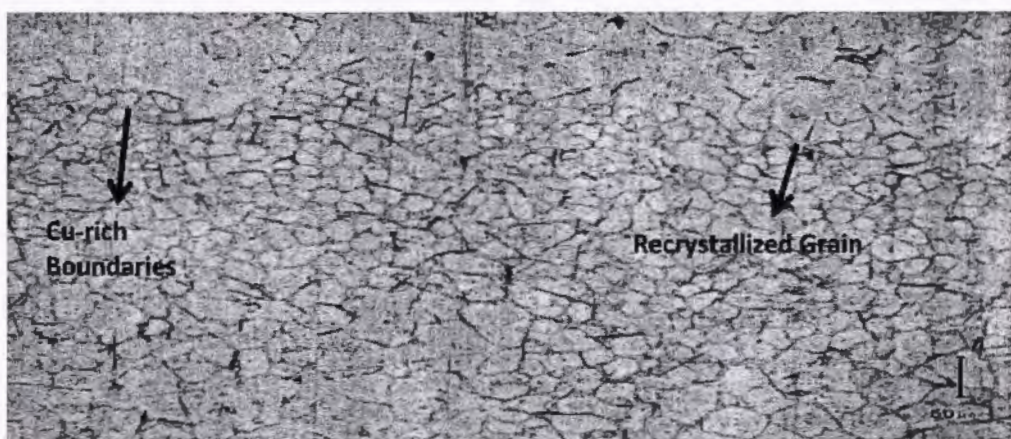
Fig. 3.10 HAZ of AA2319 filler welded base metal

During the welding process, a supersaturated solution of molten metal is formed near the welding

torch. With the passage of time, the temperature of the welded specimen decreases and the alloying components (Cu) starts to rush towards the grain boundaries. As a result of this movement, a Cu-depleted α-solid solution region is formed[38]. Due to the absence of strengthening particles i.e. intermetallic, this zone is the flimsiest zone. The detailed microstructure of HAZ is shown in figure above.

Clusters of nearly same and equal sized grain can be observed in the HAZ. This happens because of the recrystallization and Intermetallic depletion of Cu atoms from that zone. At some places in the micro structure, the deposition of Cu is found to be higher than the remaining area which accumulates on the grain boundaries of that zone. When a certain level of concentration, the grains are detached with the neighboring ones this segregation leads to the abrupt loose of mechanical properties[39].

3.4.3 Weld Nugget Zone (WNZ)

A clear and distinct solidified dendritic structure can be observed in fusion or weld nugget zone as shown in figure below. Due to the high temperature of welding process, a molten pool of metal is formed at weld nugget zone. Due to the fast cooling and solidification of welding, a metastable stage (α + Liquid) is formed. This stage exists between liquid and solidus parting. Meanwhile the second phase particles θ (Al_2Cu) starts to deposit around the already deposited and hardened α-grains where maximum solubility of the studying alloying element parallel to the solidus limit exists. The concentration of copper in both base metal (AA2219) and filler material (AA2319) is the same i.e. 6.3%. Due to that effect, the two phases "θ" and "α" instantaneously separate out as the solidification temperature drop to the solvus limit. This phenomenon is basically the major cause of deterioration in mechanical properties in this zone. Due to that abrupt mechanical changes, two metastable species of second phase particles have been formed which are donated θ′ and θ″. Both have the chemical composition of second-phased particle (Al_2Cu). They are generated with due to the successive declining of temperature[40].
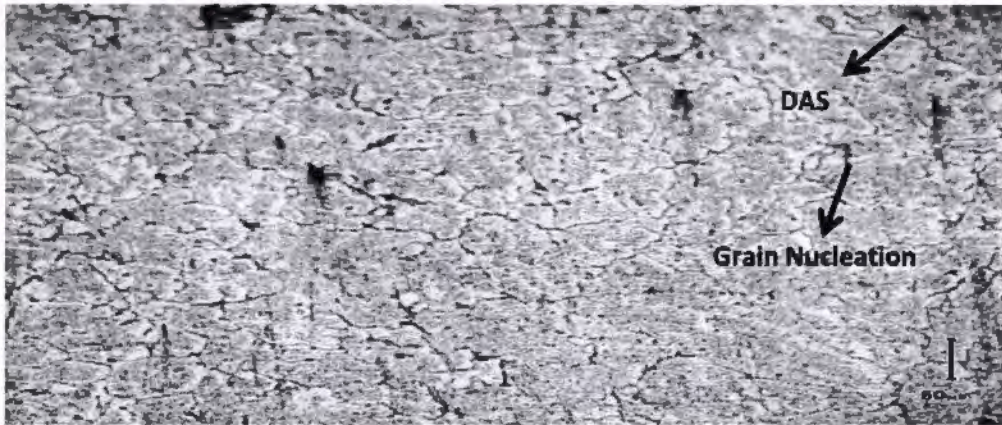
Fig. 3.11 Dendritic structures of WNZ (Filler AA2319)

The cooling has been done on room temperature which is lower than eutectic temperature. As a result of this, a eutectic network forms which can be observed around the dendritic structure.

In the weld nugget zone, due to the solidification, a grain nucleation is always introduced which leads to dendritic structure. Because of this shrinkage and presence of entrapped gases, detachments in the dendritic arm can be clearly shown and these are responsible for the delicate zone formation in this zone. These dendritic arms also facilitate the corrosion in this zone. The researchers have found that by using the AA2319 filler alloy and TIG welding, the dendritic arm spacing (DAS) reduces considerably in WNZ.

The solidification time of filler alloy or weld metal t_f is very less as compared to the base alloy. Due to that effect, there exists a much lower spacing between the adjacent feathers of the same dendrite [41].

$$DAS = 34.9 \cdot C_{cu}^{-0.333} \cdot C_{Si}^{-0.145} \cdot t_f^{0.208}$$ 3

3.5 Microstructure Evaluation (After Aging)

From the literature view, it was suggested by previous researchers that aging has a greater impact on the microstructure of the Aluminum alloys. To find out these affects, the detailed microstructure of welded and non-welded aged specimens has been studied at different zones by using Metallurgical microscope (Olympus D20) and Scanning Electron Microscope (SEM). The detailed microstructure of BM, HAZ and WNZ are discussed below in detail.

3.5.1 Base Metal

The microstructure obtained after aging of subjected aluminum alloy is shown in Figure 3.12. For deep insight, scanning electron microscopy is also performed to elucidate different phases which
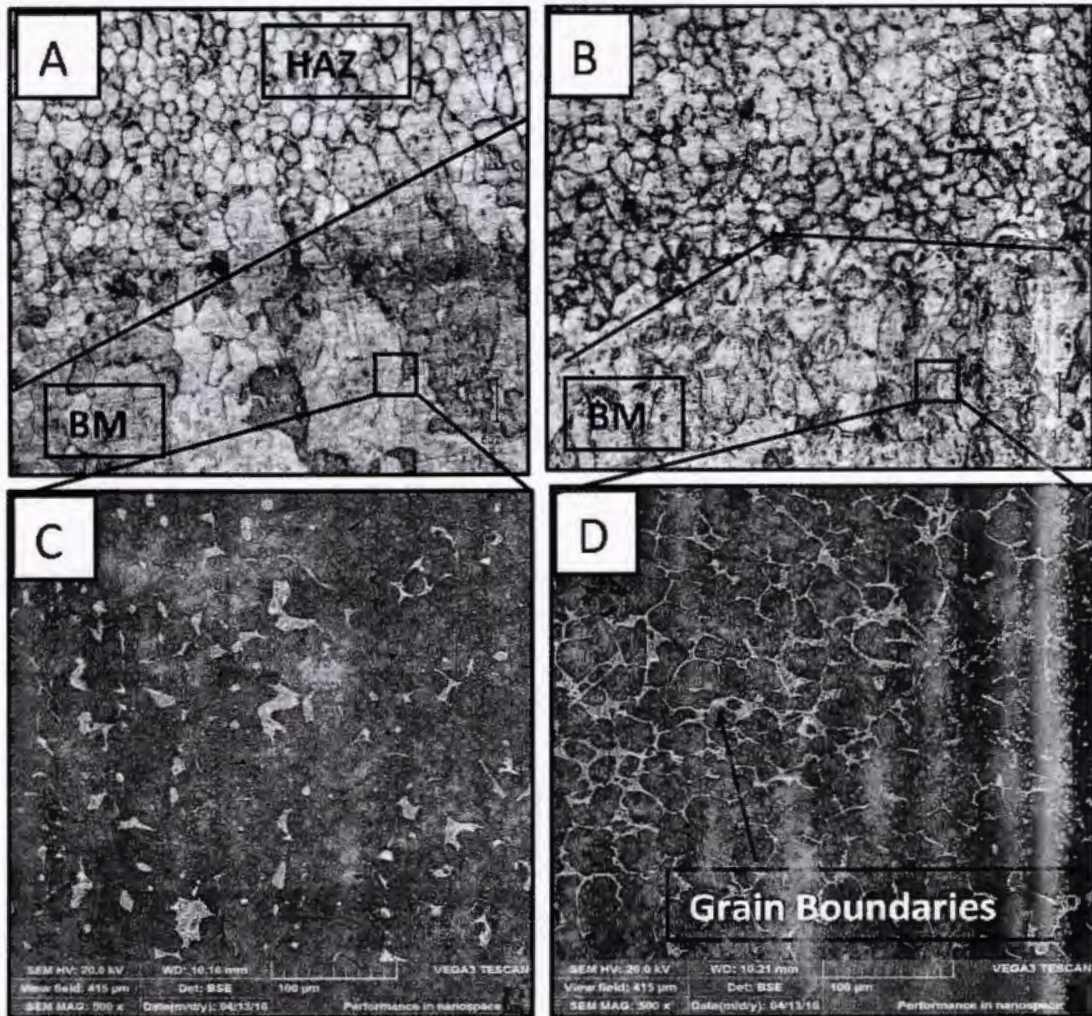
Fig. 3.12 Microstructure of AA2219 base metal after aging (a) long patched merged grains (b) base metal near HAZ (c) SEM of BM far from HAZ (d) SEM of BM near HAZ

are recrystallized after aging process. The main difference in the metallurgy of base metal before and after aging process is the diminishing of minute pseudo, grain boundaries, which ultimately turns the incomplete grains into long, flat patched grains which are shown in Figure 3.12 (a). However, the base metal zone which is in the neighboring of Heat affected zone (HAZ) shows the adverse behavior as compared to the zone which are far from HAZ. They are overlapped, inter merged and partially recrystallized small sized grains as shown in Figure 3.12 (b).

Moreover, from the obtained microstructure of aged material, we have found no evidences of secondary phase precipitates (Al_2Cu), which supports the fact that the dissolution of these precipitates is not crystalized regardless of the different zones segregated in the base metal. From Figure 3.12 (c) & (d), it is clear from the aging of the zone that the grain boundaries are more vivid near the BM/HAZ boundary as compared to the BM zone which is very far from heat source. It might be possible that it's either due to the coagulation of precipitates at the pseudo boundaries or the shrinking of peripheral area of immature grains.

3.5.2 Heat Affected Zone (HAZ)

The microstructure of aged HAZ is shown in Figure 3.13. The supersaturated solution, which is formed after welding process at HAZ, is turned into its saturation after aging process. The excessive amount of precipitates, which were forcefully dissolved into aluminum solution, are now seen at dense grains boundaries as shown in Figure 3.13 (a). The migration of Cu, from grain's interior to boundaries, is excelled due to aging. High resolution light microscopy of grain boundaries, as shown in Figure 3.13 (b), reveals that the concentration of copper can be easily judged due to light yellowish color.

Copper rich boundaries makes HAZ more fragile as compared to non-aged one. This happens due to extra brittleness of the metal at aged boundaries of HAZ. Small sized grains which originate at HAZ spreads a net of dense grain boundaries are responsible of intergranular crack propagation. Due to presence of crystallographic disarrangement near foreign particles at grain boundaries, the fatigue strength of this zone is very poor as compared to any other zone investigated in this research. From the fractography of the subjected zone, it is found that somewhere still secondary phase particles (enriched with Cu) are detected with in the grains instead of boundaries as shown in Figure 3.13 (d). These seldom appearing cuprous particles with in the grains are thought to be responsible
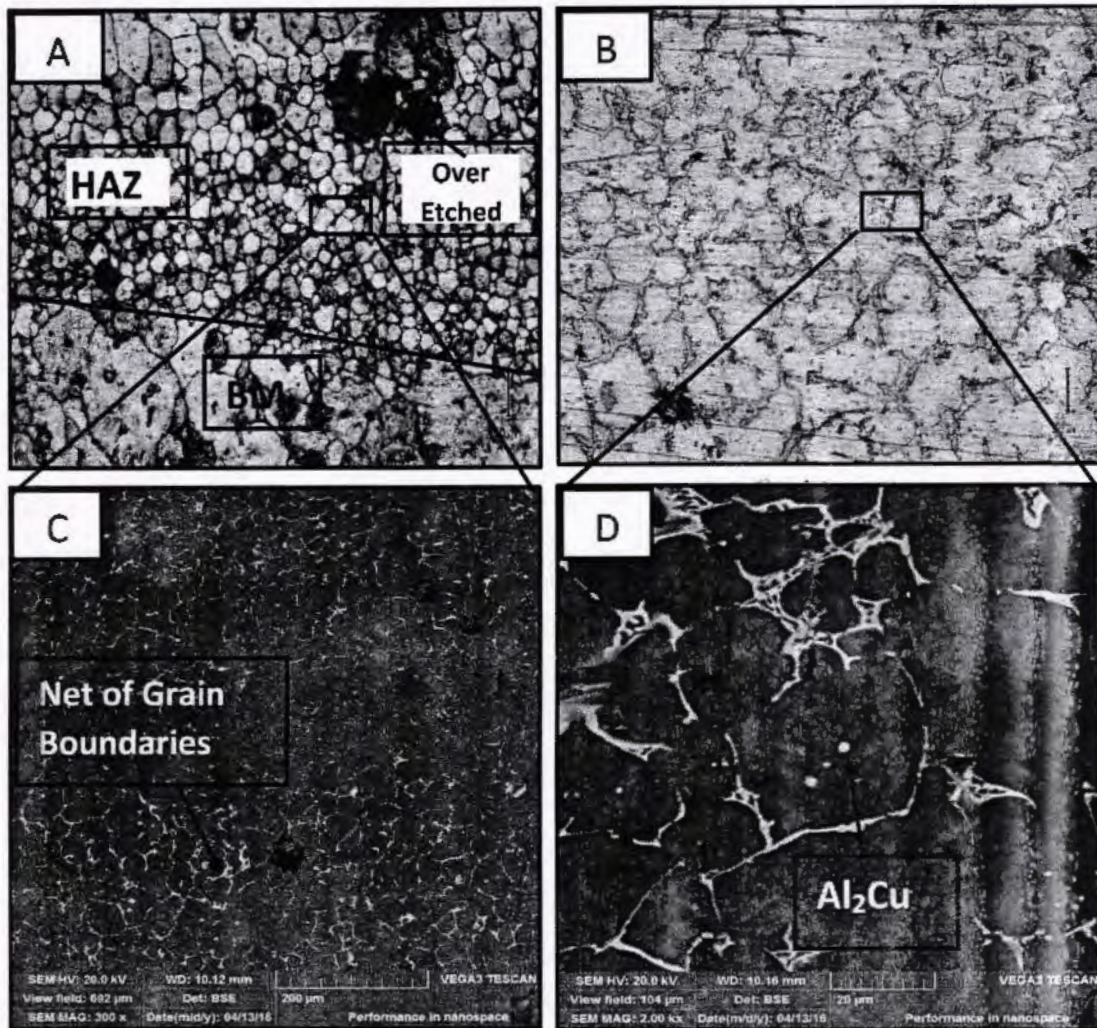
Fig. 3.13 Microstructure of AA2219 HAZ after aging (a) dense grain boundaries of HAZ (b) high light microscopy of grain boundaries (c) SEM of HAZ (d) Presence of secondary

of minute ductility which is shown by this zone. A comprehensive data acquisition system is also available which supports the automatic storage of captured metallographic pictures.

3.5.3 Weld Nugget Zone (WNZ)

From the microstructure of aged weld nugget zone, it is observed that the dendritic structure, which is obtained after welding due to segregation of α and θ phase, has been recrystallized completely. The precipitates which are arrested due to the rapid cooling of welding, started to separate out from plain aluminum contents. However, it is observed that these precipitates never shifted to boundaries due to unknown reasons (it need some more research which is not the focus point of this thesis. Authors are interested to investigate this scenario in near future). Because of this fact, proper distribution of strengthening particles become possible and this is the reason of

39

enhancement of mechanical properties of this zone as compared to the WNZ obtained after welding.
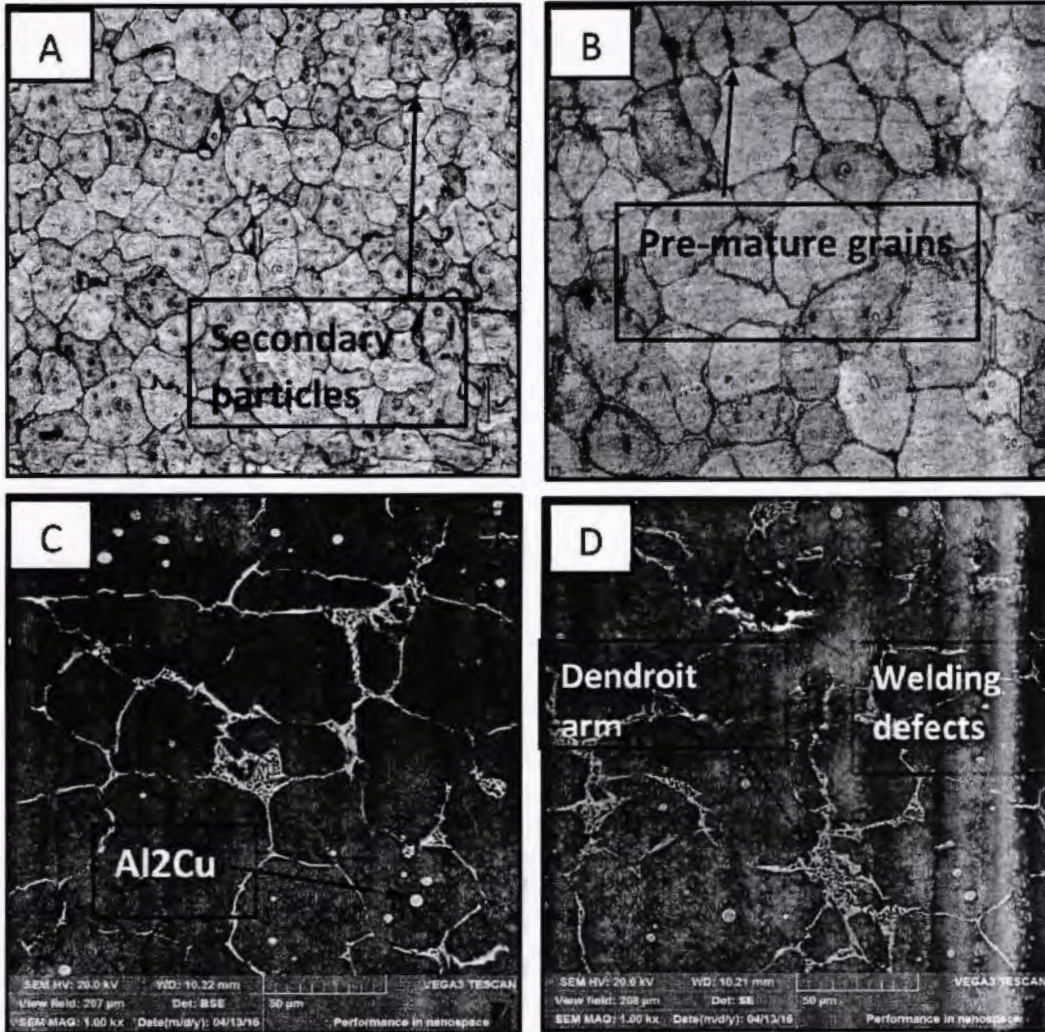
Fig. 3.14 Microstructure of AA2219 WNZ after aging (a) secondary particles in WNZ (b) Premature grains in WNZ (c) Al2Cu in WNZ (d) Welding defects and dendroit clusters

If the narrow area near the boundaries (which is still super saturated solution) is ignored, then the whole microstructure (which once stated as dendritic) is termed as mature grain as shown in Figure 3.14 (b). In other words, the specie which is obtained in this zone after aging, is somewhat in between the grains and dendrites.

From the fractography of weld nugget zone, we have also observed that after aging, the dendrite arms are merged to each other or shifted/matured to grain boundaries. This factor might be responsible of decreasing fatigue strength of this zone.

4 *Modeling of Fatigue Crack Propagation*

4.1 Introduction

In this chapter, we have tried to express the damage criteria of aged aluminum alloy on empirical and analytical bases. Usually the fatigue life is ought to have many stages.

4.1.1 Initiation of crack

➢ First, the changes take place due to the application of cyclic fatigue which later, converted into permanent change.

➢ Initially the crack produced at micro level.

➢ The amalgamation of these micro cracks was taken place after a definite crack length and then advancement of crack taken place.

➢ These micro crakes were then combined and turned into macro cracks which are termed as "dominant cracks".

4.1.2 Propagation

➢ In this stage, the dominant cracks start to propagate.

➢ When the size of that dominated, cracks crosses a certain limit, then failure of structure takes place.

The initiation of failure damage is being judged by the "total life approach" which based on the different ranges of cyclic stress (High Cycle Fatigue or HCF) and strain range approach (Low Cycle Fatigue or LCF). In general, when the specimens are smooth, the fatigue testing of low cyclic fatigue has a diminutive amount of plastic deformation along with some compressive and tensile stresses[42].

4.2 Defect Tolerant Approach

The crack propagation because of fatigue testing is mainly determined by this approach. In this approach, the testing material is already given a crack or it is necessary to find out the flaws in the material before performing the experimentation.

One the crack has been developed, a series of cyclic stresses has been allpied during the testing and it is not always necessary for these applied stresses to be within elastic limits.

When the crack has obtained certain length ,under the cyclic loading, then it is assumed that the material has reached to its specified service life N_f [43].

The service life of material corresponding to the crack propagation can be determined by the following factors

      1. Critical Crack Length, a_c

      2. Fracture Toughness, K_{IC}

However, the prediction of crack propagation can be done by only using the empirical formulas which are related to the crack growth based on fracture mechanics.

Following theories are normally used in the modeling of fatigue crack propagation

4.2.1 Linear Elastic Fracture Mechanics

This is one of the basic approaches utilized in analyzing the cracks leading to material failure. Linear Elastic Fracture Mechanics (LEFM) is used in the laws related to crack propagation that are applied in the condition of small scale yielding (SSY)[44].

In this approach the length of crack and specimen size is very much large as compared to plastic zone of crack tip. The dominant loading is pure elastic type in this method.

4.2.2 Elastic Plastic Fracture Mechanics

When the crack propagation is in the range of smart size plastic deformation then Elastic plastic fracture mechanics (EPFM) approach is used. In this method, it is common to use J-Integral. By using nonlinear, monotonic model the J-Integral value is derived[45]. This derived value is then successfully applied to fatigue crack growth (Elastic-plastic). Its parameters are mathematically path independent and feasible.

4.2.3 FCGR Variables

There are two types of variables which are basically studied for fatigue crack propagation.

    ➢ Scale

- ❖ Thickness effects on FCGR
- ➢ Conditions applied during testing
  - ❖ Applied load ratio (R) effects
  - ❖ Temperature effects

4.3 Goals of Fatigue Crack Propagation Modeling

The objective of fatigue crack propagation modeling may include many methods and approaches.

- ➢ First approach is to find out a criterion in which fatigue crack propagation should be independent of specimen's scale and all testing conditions.
- ➢ In second approach, there will be defined a criterion which is focused on a single function containing both the scale parameters and testing conditions.

The working temperature is room temperature for both types of materials and no test is held in other range of temperature however, the tested alloy is pre-heat treated. The applied load ratio is kept same R=0.1 for welded and non-welded aluminum alloy.

$$R = \frac{Pmin}{Pmax} \qquad\qquad 4$$

For comprehensive and satisfactory results, it is advised that tests should also be performed at some other load ratio (R = 0.7)

4.4 Effects of 'R' Ratio

It is generally considered that when the value of R is increases then the crack propagation rate is also increases for a specified value of ΔK. Up till now there are two types of approaches developed to consolidate the curves of fatigue crack propagation.

First method depends upon on physical features of R ratio. The main factor that is involved in this method is crack closure. And it is general concept that the value of crack closure is higher at low value of R ratio and its effects are totally negligible when the load ratio increases to a high value[46].

43

This crack closure phenomenon shielded the propagating crack for specified cycles of applied load ad it happens even for tensile loading. When this shielding is present against loading then resultantly there will be decrease in the value of applied ΔK.

When the value of ΔK decreases then definitely there will be a decrease in the rate of crack propagation. For consolidation of results under these shielding effects, it is advised that ΔK (for which the whole fatigue crack is shielded) is subtracted from the total value of ΔK.

The other method is totally principle base and empirical nature type. This approach is totally defined by mathematical methods. In this approach, it is narrated that the fatigue crack propagation rate is not only dependent on stress intensity factor. It is said that it is dependent on both, the ΔK and K_{max}[47].

For this method, there are many possible techniques and works are developed to consolidate the data. Most of the approaches are generalized up till now.

4.4.1 Crack Closure Based R Ratio Effects

It is considered that there is apparent small crack propagation rate is in Paris zone of Paris curves under the effects of R ratio on fatigue crack propagation as shown in Fig 4.1.
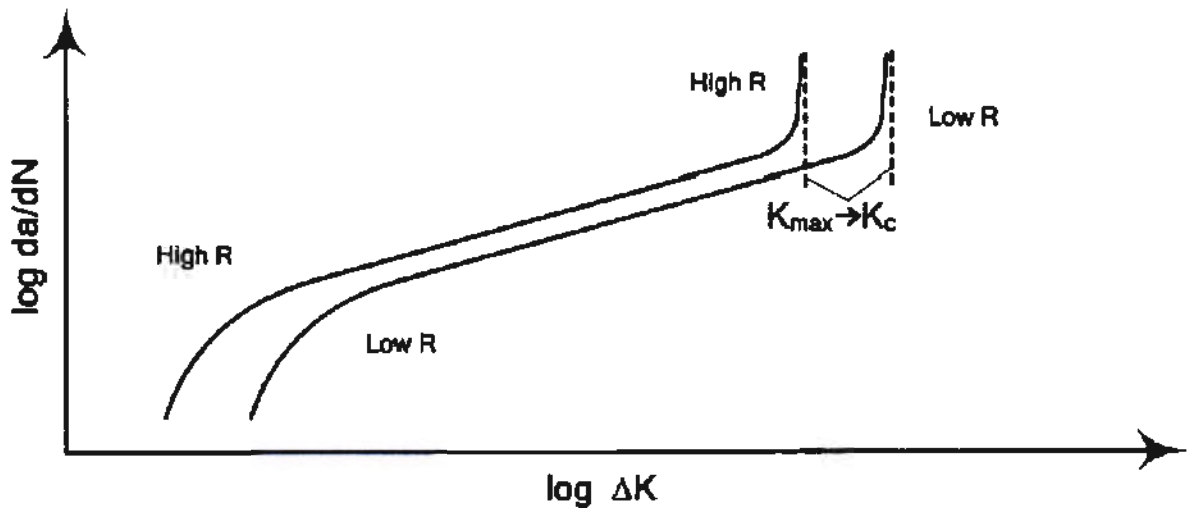
Fig. 4.1 R ratio effects on FCGR of ductile material

From the above figure, it can be concluded that the propagation of crack can be made slow by decreasing the value of stress intensity factor under the effects of crack closure. The crack closure

phenomenon has further explained in next figure, which shows a solid relationship between applied stress and crack opening displacement which is measured by strain gauge[47].

➢ The strain gauge results are shown by the line OE if the tested specimen has no previous crack. The strain gauge responses are totally elastic in nature and dependent on the Young's modulus of the tested material.

➢ In the condition when the specimen already has a crack then the zone named as A-B shows a non-varying σ- δ plot slope.

➢ The crack is starts to close at point B. Due to this crack closure there is increase in stiffness of the tested specimen.

➢ When the curve leads to point C then the value of stiffness is further increased and it happens because the length of already closed crack is increased.

➢ After some time a condition comes when the C point is totally closed and the C-D region is treated as like the solid crack free specimens.

➢ It is noteworthy that the already mentioned plot of 'σ- δ' considered as 'P- δ' plot in old literature[48].

➢ It is considered that at point B the applied stresses are termed as crack opening stresses, σ_{op}.

➢ The value of the stress which is below the limit of crack opening stress has no notable effect on the condition of crack. The reason is that the crack front is totally shielded.

➢ The matching plot is taken as a function of stress intensity factor instead of applied stress.
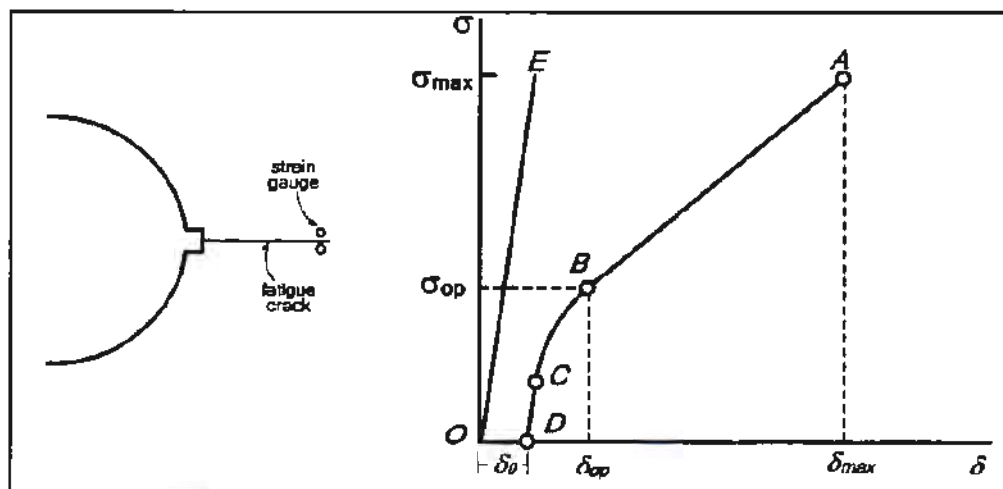
Fig. 4.2 Strain gauge measured COD and stress relationship – Crack closure explanation

4.4.2 Crack Driving Force Based R Ratio Effects

The effects of crack closure on R ratio is described due to many reasons including crack roughness, formation of oxide layers on the lips of cracks, debris and plastic regions formation at crack front. These all factors are true but crack closure is not limited to these factors and it should be fully shielded when crack opened for a complete correction, which is not always true in daily services of different parts. Many crack closure models are available in literature depending on environmental effects, partial closeness of crack, compressive stresses and residual stresses.

There is another model which has no need of account of crack closure model. In this approach, it is considered that the fatigue life of the specimen at crack initiation stage has a close relationship with the crack propagation stage. In this model the effective stress responsible for crack propagation depends on maximum value of stress along with the upper limit of applied varying stress[49, 50].

$$K = K_{max}^{1-m} \Delta K^m = (1 - R)^m K_{max} \qquad\qquad 5$$

In Eq. 5 'm' is represented as material property while 'K' is known as stress intensity factor for positive R value of the fatigue crack propagation data consolidation.

As it is previously mentioned that load ratio effect may be due many known and unknown reasons and it is also not necessary that these depend on material properties. So, it is possible to replace 'm' by 'α'.

After replacing 'm' by 'α' the eq. is changed into;

$$K = (K_{max})^\alpha (\Delta K)^{(1-\alpha)} \qquad\qquad 6$$

The sensitivity of 'K' is measured on 'K_{max}' when the conditions of above equation is$0 \le \alpha \le 1$. The 'α' depends upon many parameters like as environmental effects, material properties and specimen thickness.

The effective stress intensity factor can be explained by taking two different assumptions.

➢ At crack tip the damage is due to two mechanisms which are simultaneous in nature. One is based on monotonic damage and second is based on cyclic damage. These are due to K_{max} and ΔK respectively.

46
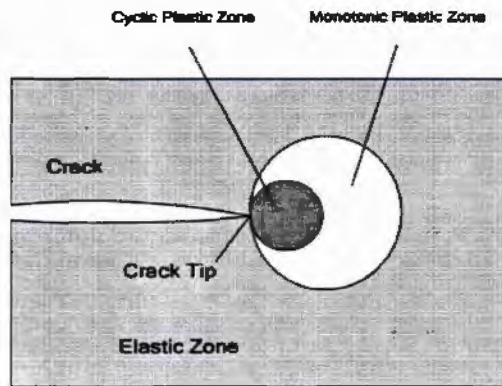
Fig. 4.3 Different zones formed at crack tip [43]

> In the zone where $K_{max} > 0$ and the tensile stresses are also existing in that zone then the necessary condition of fatigue crack propagation is fulfilled.

4.5 Crack Branches

When the fatigue crack propagation takes place then it is not necessary that single geometric disorder become a fatigue crack at large scale and become the cause of specimen failure. Some times while the crack propagation takes place then the crack tip may divided into many branches that's called crack branching[6].

In this work the crack branching is also takes place. The characterization of branching is described below:

> Branching takes place at both positions i.e. from the parent crack tip and from another portion of parent crack other than tip.

> Crack branching takes place in both types of material welded and unwedded, but it is observed that the concentration of crack branching is more in welded aluminum alloy than the base metal.

> It is observed in welded AA2219-T87 that these branches propagate following the grain boundaries (intergranular).

> The formation of oxide layers between the weldment is also cause of crack branching.
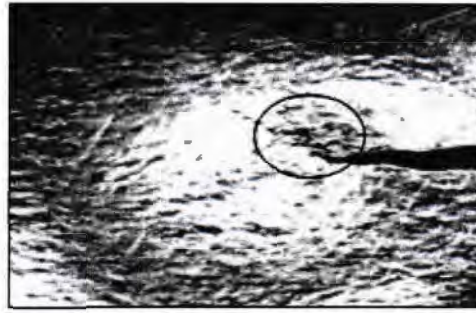
Fig. 4.4 Crack branching in AA2219-T87

4.6 Finding the Value of ΔK & da/dn

During the fatigue testing on MTS-810, the data acquisition system provides the crack length along with its corresponding applied cycle. From a series of crack lengths along with their cycles, each parameter is subtracted from its next greater value. The results obtained from two subtractions are divided accordingly to obtain da/dN.

$$\frac{da}{dN} = (a_{max} - a_{min})/(N_{max} - N_{min}) \hspace{3cm} 7$$

While the stress intensity factor is find by using the following formulae

$$K = \left(\frac{P}{B\sqrt{W}}\right).f(\frac{a}{W}) \hspace{4cm} 8$$

f (a/W) is called geometric correction factor[51] and it is totally dependent on fatigue crack length to specimen width ratio;

$$f(\frac{a}{W}) = ((2 + \frac{a}{W})(0.886 + 4.64\left(\frac{a}{W}\right) - 13.32\left(\frac{a}{W}\right)^2 + 14.72\left(\frac{a}{W}\right)^3 - 5.6\left(\frac{a}{W}\right)^4)/(1 - \left(\frac{a}{W}\right))^{3/2} \hspace{1cm} 9$$

Where,

P = Applied Load

W= Width of specimen

B = Thickness of the specimen

a = Crack length

48

5 *Results & Discussions*

In this chapter, a detailed discussion has been done about the results of all tests performed in this research work. Two types of tests are being conducted in this research which are are:

1. Hardness Test

It is another type of tensile test in which hardness of welded metal is investigated. The main objective of conducting this test is to check the fragileness of different zones which are formed after TIG welding.

2. Fatigue Crack Propagation

The behavior of fatigue crack at room temperature has been studied in this test for welded and un-welded CT specimens. It is necessary to explain here that all tests are conducted on pre-heat treated metal.

Along with these tests the post-mortem analysis of cracked surface and the path followed by the crack with respect to microstructure is also enlighten.

5.1 Hardness Test (Before Aging)

A detailed micro-hardness test has also been done to measure the hardness number of naturally aged specimen at different weldment zones formed during the TIG welding.

5.1.1 Formation of Different Weldment Zones

As the flame temperature of TIG welding torch is above 2000 °C and aluminum is non-ferrous soft metal, so during welding process the metal under the torch is totally melted and as the torch passed away then rapid recrystallization takes place. The zone adjacent to this melted portion is also changed due to its properties variations.

5.1.1.1 Base Metal

> ➤ This zone has the highest Brinell hardness number with respect to competitive ones.
>
> ➤ As the hardness number is checked while the pre-heat treatment process is completed so the effects of T87 heat treatment also affect the hardness number of original base metal.
>
> ➤ The reason of high hardness number is due to presence of high amount of α-Al, however some amount is disturbed while performing pre-heat treating.

> The intermetallic are arranged in such a manner that they are providing the maximum strength to base metal.

> As it is very far away from heat source so the effects of welding temperature are very negligible on this zone.

5.1.1.2 Heat Affected Zone

Heat affected zone (HAZ) is formed between two different zones named as base metal and weld nugget zone.

The hardness characteristics about this zone are described below:

> The hardness number of this zone is greater than weld nugget zone while lower than the base metal.

> The thickness of this zone is totally varying from notch tip of the CT specimen to the end of the specimen as shown in figure below.
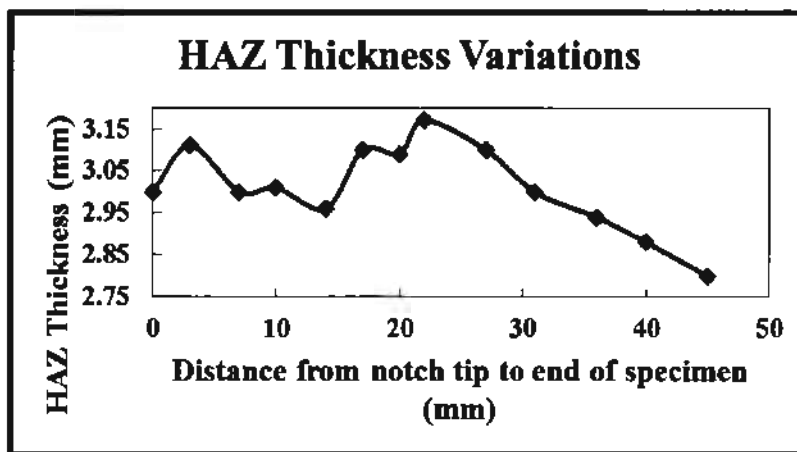
Fig. 5.1 HAZ Thickness variations in CT specimen

> In this zone the hardness number is suddenly lost due to improper recrystallization of semi-melted portion of metal.

> The readjustment of second phase particles in this zone is not helpful to provide proper strength to the subjected alloy.

> Due to high temperature, the main alloying component, Cu, is melted and move away from this zone to molten pool of weld nugget zone causing the strength decrement of this zone.

5.1.1.3 Weld Nugget Zone

It is the most important area of weldment because it is the real joint portion of two bulk materials. This zone is created by a molten pool of base metal and filler alloy. The hardness characteristics of this zone are described below:

➤ It is the most fragile zone having the lowest hardness number as compared to other competitive zones.

➤ In this zone the recrystallization of molten metal pool is taken place very quickly.

➤ During rapid recrystallization of grains the strengthening particles failed to find proper positions in grain structure.
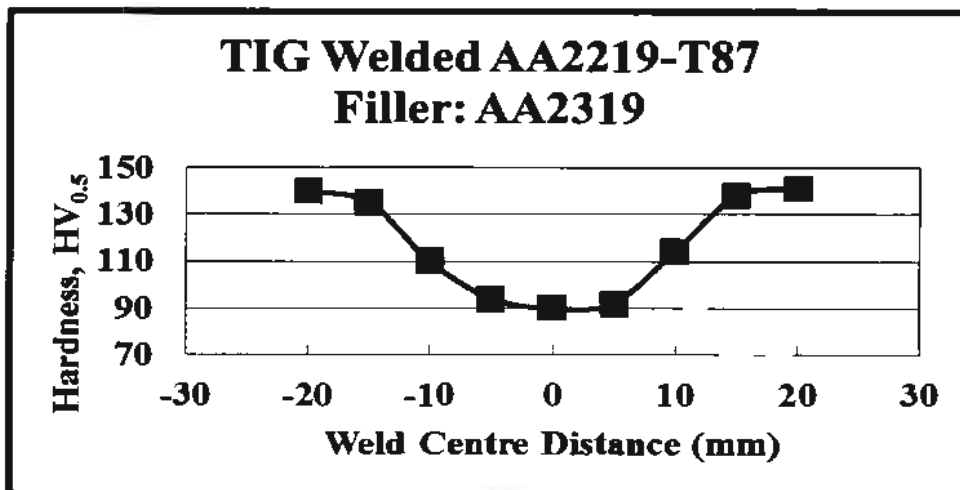
Fig. 5.2 Micro hardness of TIG welded AA2219-T87

➤ In this zone, some secondary particles concentrate on grain boundaries are also helpful in decreasing the hardness of the WNZ.

➤ There is dendritic structure is formed after recrystallization in this zone and as the dendritic structure depicts the softer area so resultantly this zone has lowest hardness number.

5.2 Hardness Test (After Aging)

The considerable variations in hardness after aging of Aluminum weldment are detected in heat effected zone and fusion zone. This is because the impact of welding heat is more prominent in above mentioned zone. From the fig.5.3 shown below, it is concluded that the hardness of the HAZ and FZ has increased after aging process. The main cause of this increase in hardness is due to the

availability as well as distribution pattern per unit volume of second phase strengthening precipitates.

Another factor for the higher hardness values in fusion zone after aging as compared to the plain aluminum is due to the incorporation of the copper on the upper surface and this presence at the surface area of the weldment is responsible for the high hardness values.
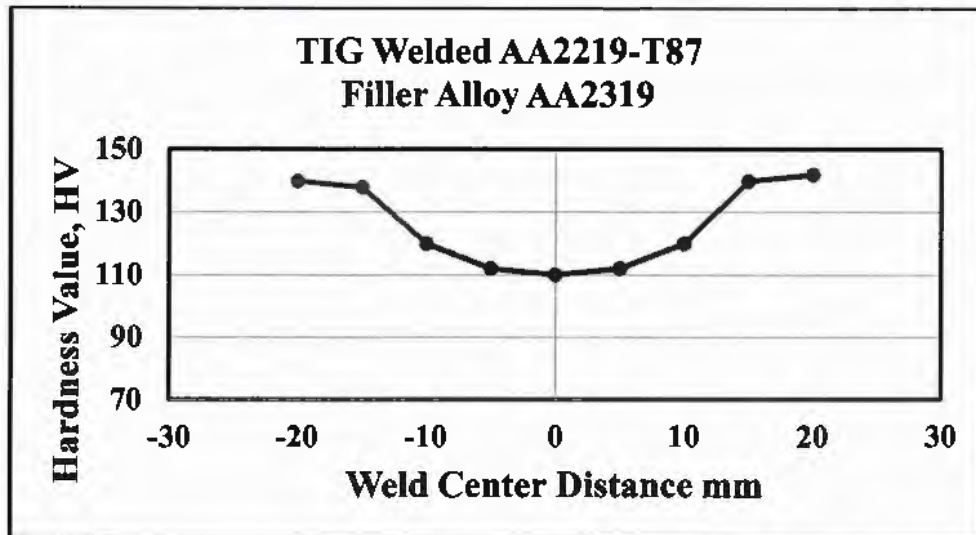
Fig. 5.3 Micro hardness of TIG welded AA2219-T87 after natural aging

5.3 Fatigue Test

Due to continuous application of cyclic load, the material encountered by fatigue weakens. Under these continues and locally generated loading, the material undergoes a specific failure type. The best thing about the fatigue crack generation is that it happens at a stress level which is much lower than the yield stress.

When the cyclic loading and unloading crosses the safe limit, named as threshold limit, the crack generation takes places at microscopic level. The fatigue cracks are basically started from a point where the concentration of stresses takes place like as grain interfaces; persistent slip bands (PSBs), notches and sharp corners.

As the crack starts generating, it propagates very quickly and leads to the catastrophic failure.

5.3.1 Prominent Scientists Worked on Fatigue

➢ Sir James Alfred Ewing – Fatigue failure origin at microscopic crack

➢ O. H. Basquin – On wholer's test data proposed a log-log relation for S-N curve

➢ A. M. Miner – Linear damage hypothesis

➢ A. Palmgren – Linear damage hypothesis

➢ L. F. Coffin – Explains fatigue Crack Growth Rate (FCGR) with respect to crack tip plastic strains.

➢ P. C. Paris – Provide famous Paris's law about fatigue crack growth rates.

➢ W. Elber – Explains the mechanism of Fatigue Crack Closure

5.3.2 Fatigue Crack Propagation Stages

According to fracture mechanics, the fatigue failure can be divided into its four sub categories [52].

- Nucleation of crack
- Crack growth; Stage I
- Crack growth; Stage II
- Failure of specimen
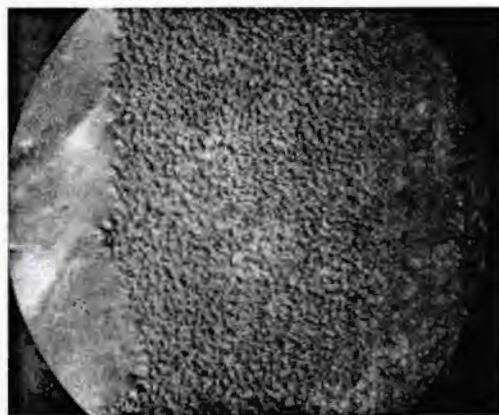
Fig. 5.4 Fatigue failure representation at different stages

Firstly, the crack nucleate at some stress raiser point then the crack propagation takes place at two different stages and finally the sudden fatigue failure takes place as shown in figure below. However, in present research the fatigue crack nucleation and propagation is too minute to

describe. But these regions are differentiable when observed under microscope having high magnifications. Most of the visualized region in broken welded specimens is sudden brittle failure region.

5.4 Relation between f (a/W) and a/W Before Aging

5.4.1.1 Geometric Correction Factor for Base Metal

The f (a/w) is called geometric correction factor. Its relation is determined with respect to ratio between "a" and "w". The correction factor is calculated from the formula of stress intensity factor under the load of "F"[53].

$$K1 = \sigma\sqrt{\pi a}.\, f\left(\frac{a}{w}\right) \qquad\qquad 10$$

This relation is calculated for CT specimen having H/W = 1

From Fig 5.5 it is elaborated that there is linear relation between geometric correction factor and ratio of crack length to specimen width. The linear relation in Figure 5.5 that there is uniformity in material microstructure up to satisfied level.
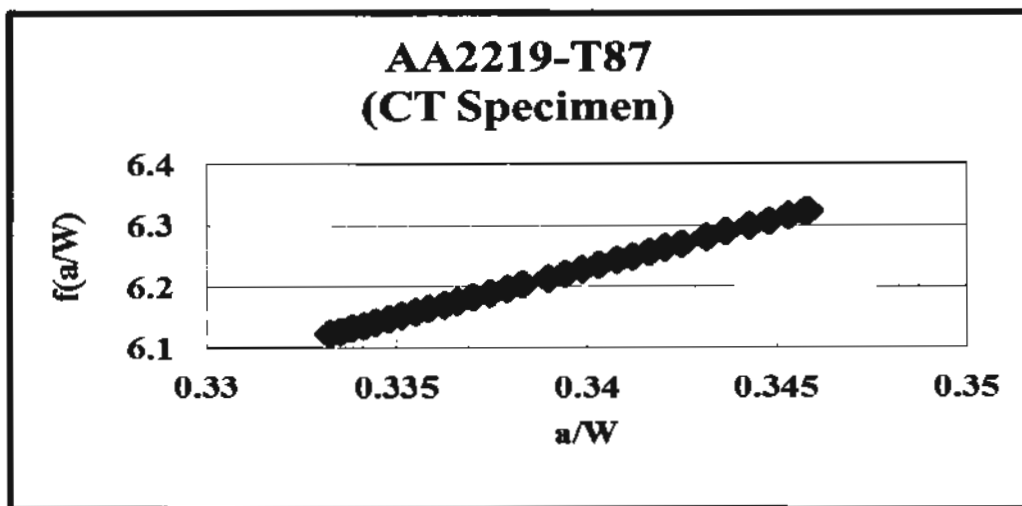
Fig. 5.5 Relation between f (a/w) and a/w for non-welded CT specimen

5.4.1.2 Geometric Correction Factor for Welded Metal

It is observed that the geometric correction factor behavior with respect to crack length to specimen width ratio of welded specimens before aging are not same as for the base metal which depict that there are some structural changes takes place after welding of the subjected material. From the previous test results of without natural aging, it can be concluded that initially there is linear relation between geometric correction factor and a/w. At start the line is less steep with respect to base metal respective line but from mid-point it is considered that the steepness of the welded and non-welded specimens is the same as shown in Fig 5.6.
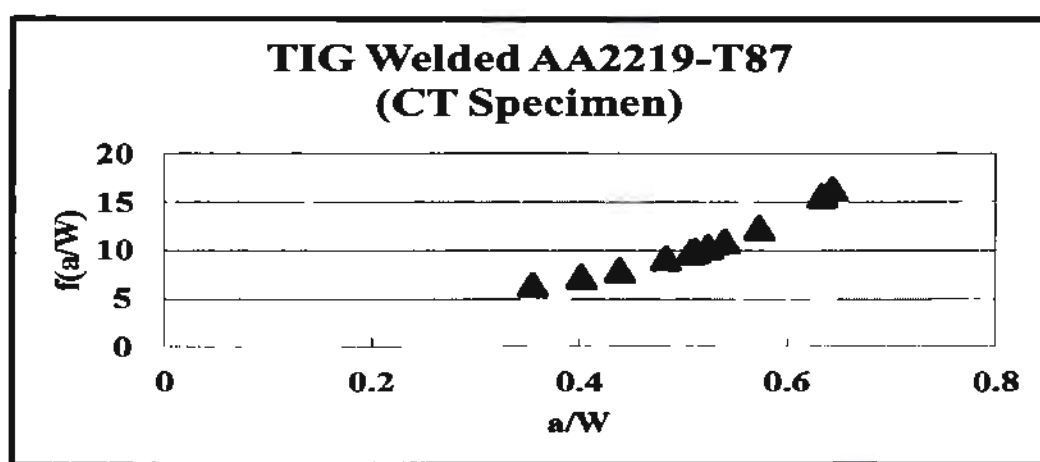
Fig. 5.6 Relation between f (a/w) and a/w for welded CT specimen

The nonlinear behavior shows that the crack propagation trend is varying in TIG welded specimen during the test. As the crack propagation behavior varies then definitely the geometric correction factor also varies because it is the function of "a/w". This relation is calculated at "H/W=1" of welded specimens.

5.5 Relation between f (a/W) and a/W after Natural Aging

5.5.1 Geometric correction factor for base metal

As the geometry of the specimen which are used for fatigue resting before and after aging is the same, it is proposed that the geometric effects are not the contributing factor in varying the fatigue results after aging.
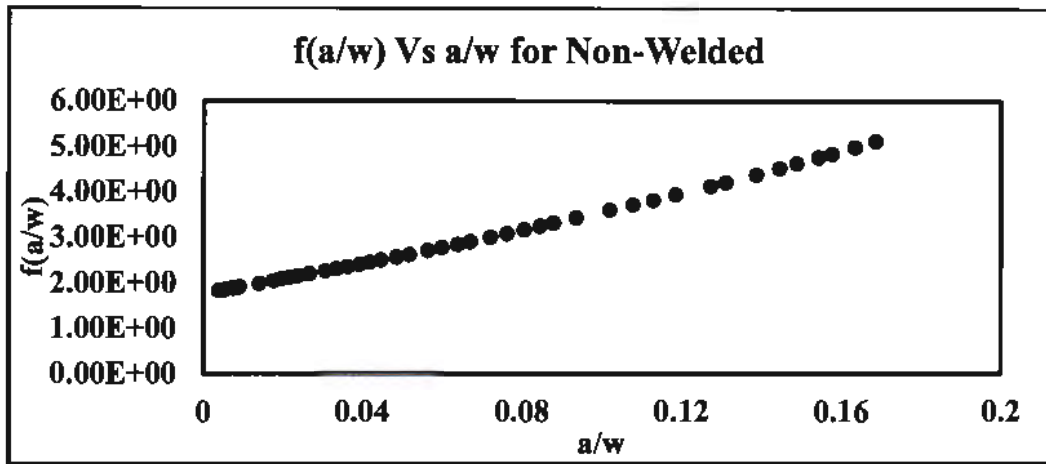
Fig. 5.7 Relation between f(a/w) and a/w for non-welded CT specimen after aging

However, for the sake of extra care and results accuracy, geometric factor effects are verified in Figure 5.7 & Figure 5.8. From the below mentioned figure, it is revealed that for base metal, the geometric effects are almost equivalent to zero. The slope of line is almost the same in aged and non-aged base metal.

5.5.2 Geometric Correction factor for Welded Metal
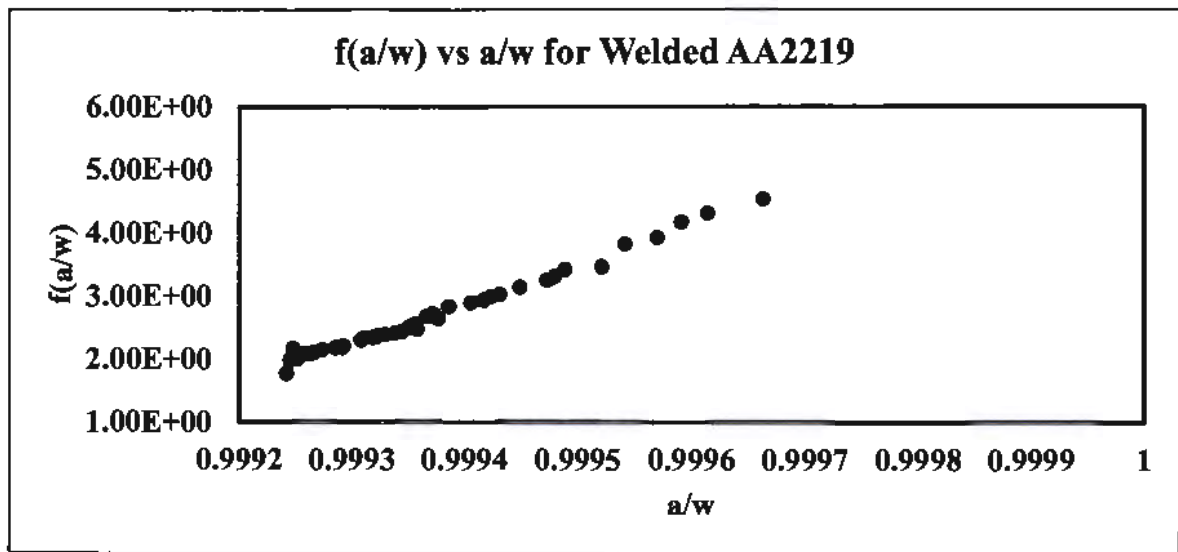
Fig. 5.8 Relation between f(a/w) and a/w for welded CT specimen after natural aging

The relation between f (a/W) and a/W for welded CT specimen after natural aging is shown in Figure 5.8. The extra linearity of obtained curve which is shown, however, in welded metal, the initial non-linearity of the curve is due to the minute variations incorporating parameters instead of the geometric factors.

5.6 Dependence of ΔK on "a/W" Before Aging

5.6.1 Base Metal

The values of stress intensity factor are calculated for both the welded and non-welded specimens. The procedure to find out the value of "Kq" is briefly described in previous chapter. The relation between critical stress intensity factor and ratio between crack lengths to specimen width is shown in Figure 5.9.
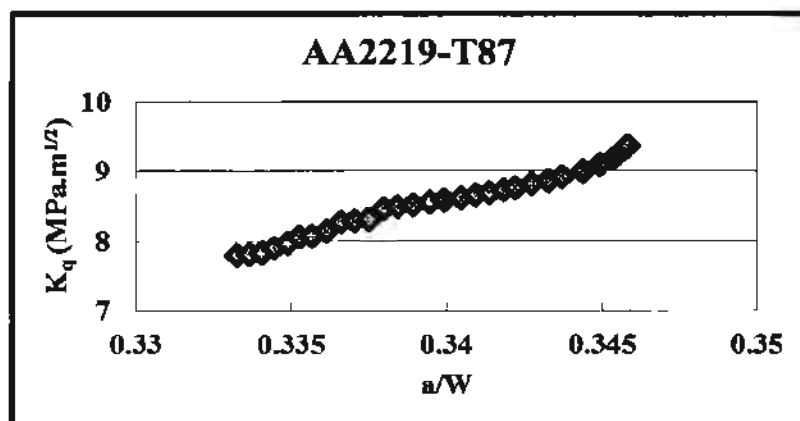
Fig. 5.9 Kq dependence on "a/w" for un-welded specimens

Critical stress intensity factor shows a clear dependence on the crack length to width ratio a/W. The dependence ratio is in the range of 0.333 < a/W < 0.347 which is in the limit of ASTM general standards recommendations, 0.3 < a/W <0.6[51]. The dependence curve of Kq is steeper from 0.333 to 0.338. However, the steepness of curve is relatively low from 0.338 to 0.347. The dependence of critical stress intensity factor increases as the "a/W" value increases in the whole trend. Before fracture for a very small period the dependence, rate is suddenly increases for non-welded base metal.

5.6.2 Welded metal

As the critical stress intensity factor depends upon "a/W" in this research so it means it depend upon the fatigue crack propagation behavior. The dependence ratio should be changed when the crack propagation trend is changed as observed in base metal and TIG welded aluminum alloy compared with each other. The relation between critical stress intensity factor and ratio between crack lengths to specimen width is shown in Figure 5.10.
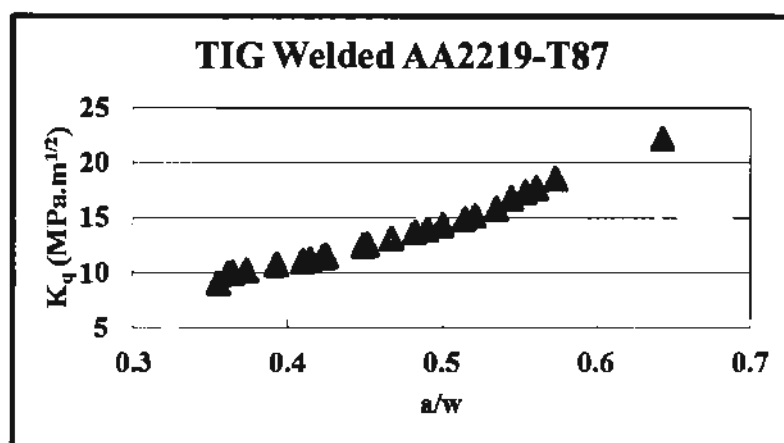
Fig. 5.10 ΔK nom dependence on "a/w" for base metal specimen after aging

It has also mentioned in literature that Kq also depend on thickness of the specimen but in this research the thickness value is kept constant for both, the welded and un-welded specimens so that results are The dependence of stress intensity factor on "a/W" is same from 0.35 < a/W < 0.47 but it minutely increases after the value of 0.47. Most of the values are in range between 0.3 < a/W < 0.6 as recommended by ASTM standards, however some data are observed out from this range due to unknown reason. The a/W range on which Kq depends for welded metal is higher than the un-welded metal.

5.7 Dependence of ΔK on "a/W" after Natural Aging

5.7.1 Base Metal

The dependence of critical stress intensity factor on propagating crack length to specimen width ratio is more prominent in after aging results as shown in figure 5.11. The obtained results of base metal after aging remained within the standard recommendations mentioned below.

It is easily observed from below figure that critical stress intensity factor dependence is finding itself more reliable after aging as there is no kink in the middle stream of the curve and the data reinforcement is in harmony as compared to the non-aged base metal.
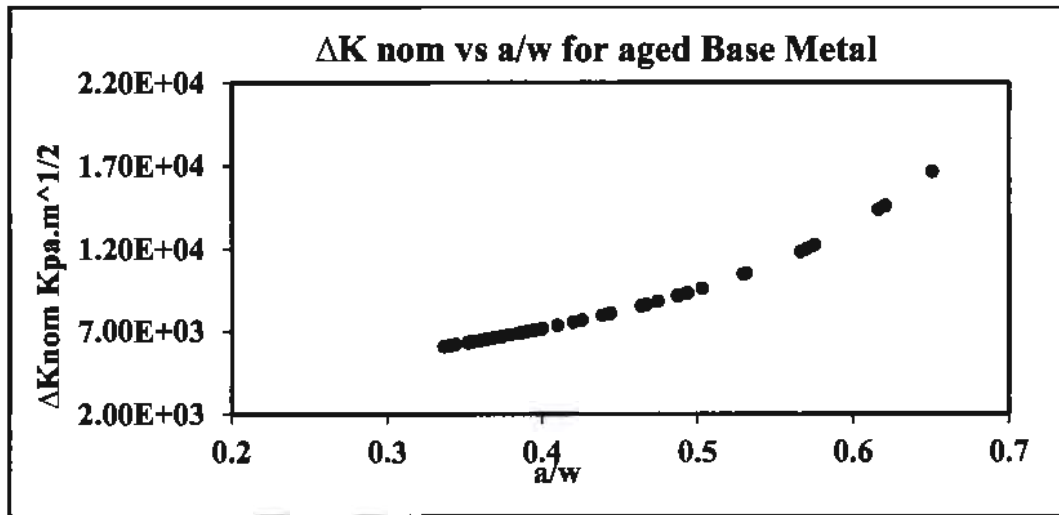
Fig. 5.11 Kq dependence on "a/w" for non-welded specimens

5.7.2 Welded metal

The comparison of K dependence on a/w is not efficiently describe while considering only mechanics based observations. Because with respect to the data plotted before and after aging of welded metal, one can only conclude that the K dependence is more efficiently predicted in after aging scenarios as compared to the previous ones.
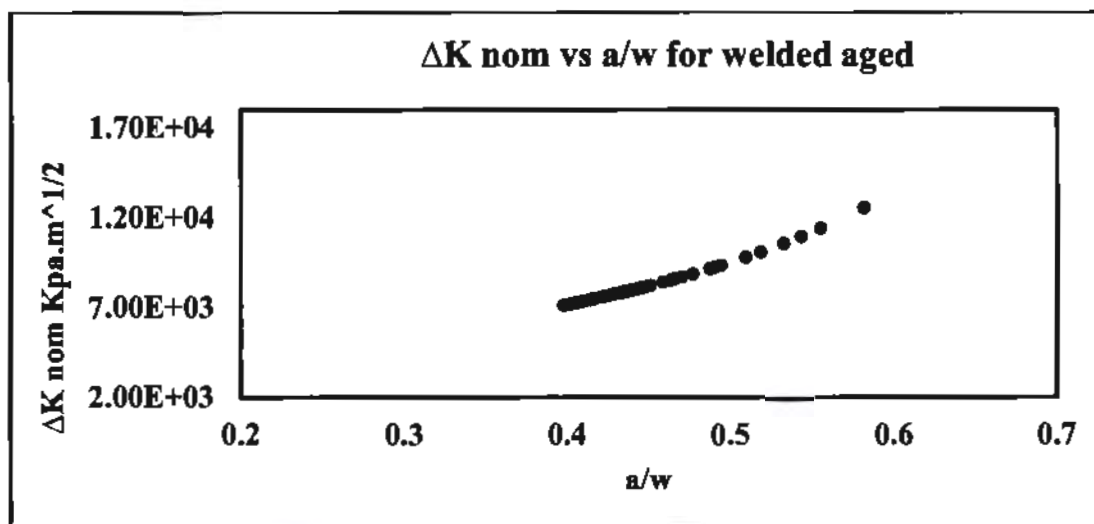
Fig. 5.12 ΔK nom dependence on "a/w" for welded specimens

The comprehensive details can only be provided while considering the metallurgical approach. As the second phase precipitates, which are maturely oriented at their equilibrium sites, reinforce after aging so this is the main reason of uniform dependence of K on a/w in this case as compared to non-aged metal.

5.8 Comparison of ΔK and a/w for Welded and Non-Welded (After aging)

Comparison of both welded and welded specimen after natural aging has been shown in the figure 5.13. A brief comparison of both graphs of f (a/w) vs a/w for welded and non-welded after aging can be done by seeing the above fig5.13. The details of individual graph have already been discussed in detail above.
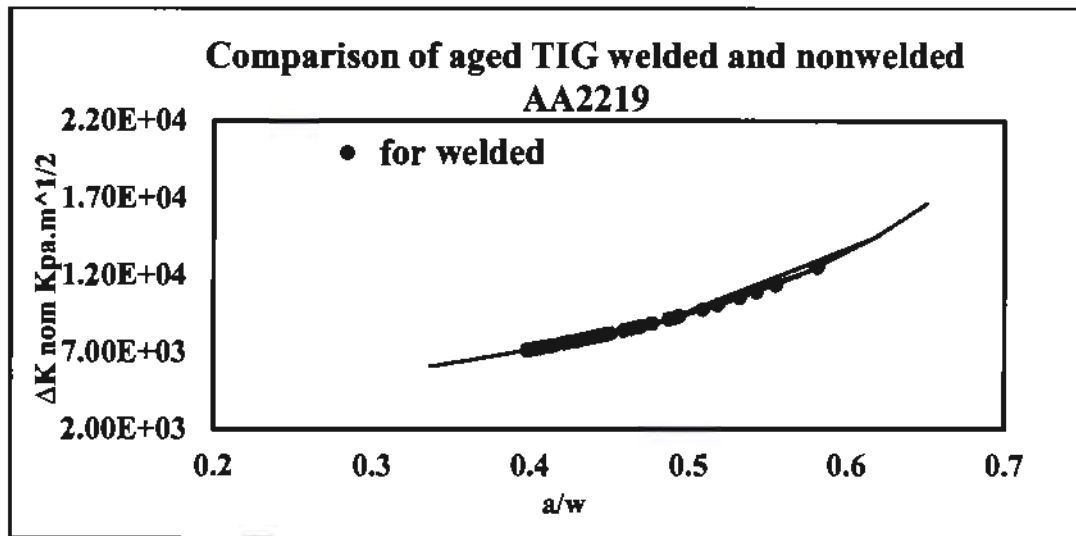
Fig. 5.13 ΔK nom dependence on "a/w" for welded and non-welded specimens

5.9 Paris Law

The most widespread law for determining the fatigue crack growth rate represented in fracture mechanics is the Paris's law[6]. It covers the fracture mechanics and material sciences technology. It relates the fatigue crack propagation in stress regime with stress intensity factor. It is represented as under;

$$\frac{da}{dN} = C\Delta K^m \qquad\qquad 11$$

Where, on the left-hand side of equation,

"a" is the crack length and

"N" are the number of cycles

Whereas da/dn indicates the number of crack opening to the number of load cycles. On the other side of the equation, "C" and "m" are constants totally dependent on material type and "ΔK" is stress intensity range, a difference of stress intensity factors at maximum and minimum loading conditions.
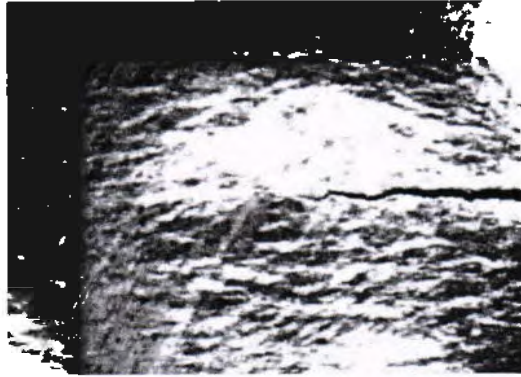
Fig. 5.14 Fatigue crack opening at Pmax.

The mathematical definition of stress intensity factor can be described as;

$$K = \sigma Y \sqrt{\pi a} \qquad\qquad 12$$

On the right-hand side of the equation, "Y" represents a dimensionless constant while "σ" is quantity of stress perpendicular to crack surface.

By substituting the value of stress intensity factor into Paris's law

$$\frac{da}{dN} = C\Delta K^m = C(\Delta\sigma Y \sqrt{\pi a})^m \qquad\qquad 13$$

When there are small fatigue cracks, then it is assumed that "Y" did not depends upon the value of crack length then the above-mentioned equation can be solved by using the methods of separation of variables.

While describing about the joints of alloys, it is more useful to explain Paris's law based on fracture energy instead of stress intensity factor.

In this research the fatigue model using stress intensity factor instead of fracture energy is used by assuming the specimens of infinite length[54].

5.10 Paris Curve

To follow the Paris model of fatigue crack growth rate, a typical type of curves is drawn per law's limitations.

The Paris curves drawn in this research have the following characteristics:

- The curves are drawn on log-log scaled paper
- Stress intensity factor is represented on the X-axis of the curve
- Y-axis of Paris curves represents the fatigue crack propagation rate per increasing number of cycles
- The curves are drawn by keeping the load ratio R= 0.1 for both welded and non-welded, naturally aged and non-aged specimens
- The frequency rate has kept 20Hz during crack propagation of both type of the specimens
- For crack initiation, each specimen takes infinite number of cycles to initiate a fatigue crack
- The most visualized portion of the curve is "fatigue crack propagation" zone, which is mostly an inclined line in case of aluminum
- The fatigue failure required just a few numbers of cycles in both cases, welded and non-welded aluminum specimens.
- The failure phenomenon may be different between in welded and non-welded specimen.
- Comparison of Paris curves for both welded and non-welded, before and after aging has been done in this research.

5.10.1 Paris curve Before Aging

5.10.1.1 Base Metal

The non-welded specimens before aging had been tested on servo hydraulic machine and they were calculated. The data obtained from machine and optically taken was organized. Then, Paris curves were drawn by utilizing both types of data on the same graph.
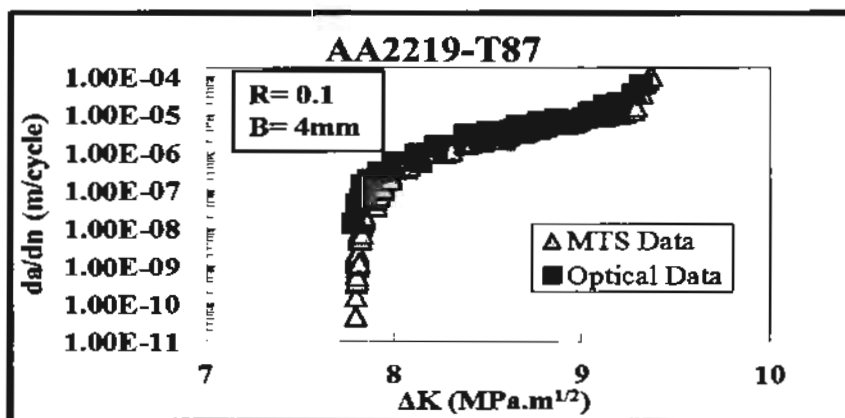
Fig. 5.15 Paris Curves for base metal

Optical and Machine Data Mismatching

Initially crack initiation required many cycles which are depicted from Paris curve formed from machine data. There is negligible difference between optical data and machine data for base metal during the crack propagation and failure of the specimens. For design purpose, the Paris curve obtained from optical data is more reliable instead of machine data [55].

5.10.1.2 TIG Welded

After TIG welding there are some internal structural changes are taken place in the metal. The positive point is that the mismatching between optical and MTS-810 data is near about zero as compared to base metal. The fatigue failure of base metal is completely ductile type, as the specimen is not completely parted off during the test. While the failure of welded aluminum alloy is totally brittle nature as the specimens are parted off with opposite machine clevis.
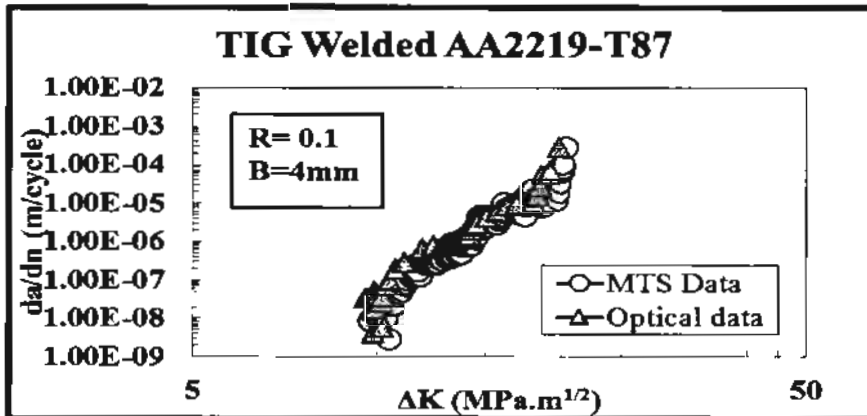
Fig. 5.16 Paris Curves for base metal

5.10.2 Paris curve After Aging

5.10.2.1 Base Metal

As Aluminum is a soft metal as compared to steel and other ferrous metals, so we are unable to obtain its endurance limit. This softness of the tested alloy and the alloy composition of as received aluminum sheets show a weird behavior after aging process in non-welded cases.

From the comparison of results show in Figure 5.15 & 5.16 it can be concluded that after aging process, the base metal has shown extra softness against cyclic loading.
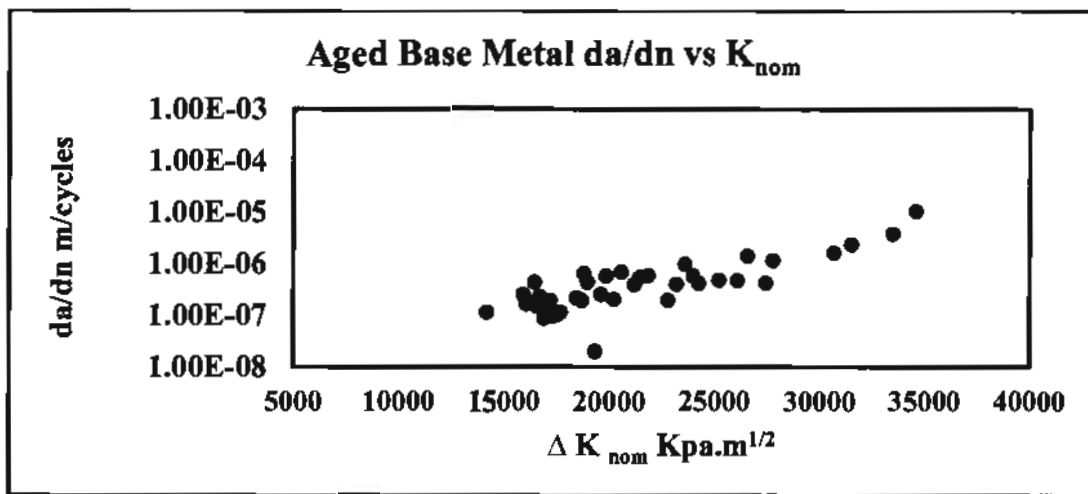
Fig. 5.17 Paris Curves for base metal after aging

It is proposed that the data scattering and discussed softness is due to the disturbance of alloy balanced percentage or some unusual chemical reaction or mechanical mixtures between the trace elements of the subjected metal.

However, it is strongly recommended for future researcher that a deep investigation should be conducted to explore the solid reason of this non-trivial behavior of soft metals after aging.

5.10.2.2 Welded Metal

From the comparison of the fatigue strength results of the welded aluminum before and after aging, as shown in figure 5.17 & 5.18, it is clearly shown that after aging, the resistance against fatigue crack growth has increased enormously. The vivid reason of this behavior is the uniform

distribution of second phase strengthening particles within the grain and at the grain boundaries. This hindrance in crack propagation is equally available in the case of intergranular as well as trans-granular failures. There is another reason of strengthening of aged metal is the maturing of Al_2Cu particles which were available above the eutectics equilibrium points. This phenomenon is responsible for extra availability of strengthening particles per unit volume of the weld metal. Form the fig 5.18, it is observed that maximum numbers of cycle are consumed in the intermediate section of the curve which shows that fatigue crack initiation and propagation becomes difficult in aged metals and this factor supports that the uniform distribution of strengthening particles is not only on the surface area which was under examination during microscopy but present three dimensionally in the whole cross section of the joint.
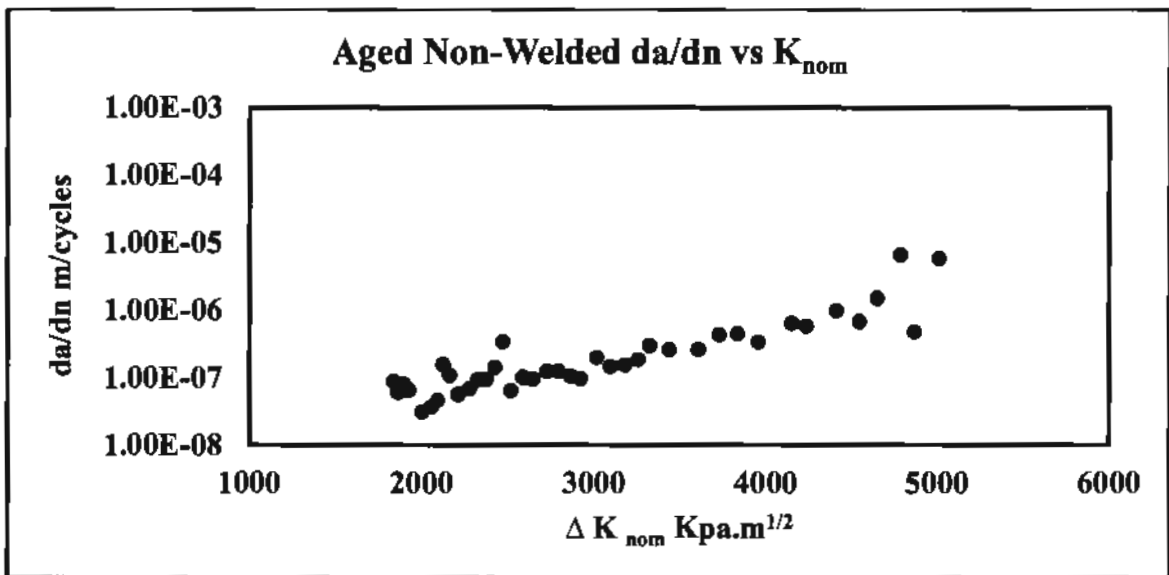
Fig. 5.18 Paris curves for TIG welded AA2219-T87

5.11 Comparison of Paris Curves (Before aging)

5.11.1 Before Aging

In crack propagation zone, it is observed that there is some minute mismatching between optical and machine data [55]. The reasons of mismatching of both Paris curves are unknown and a research task for further investigation.
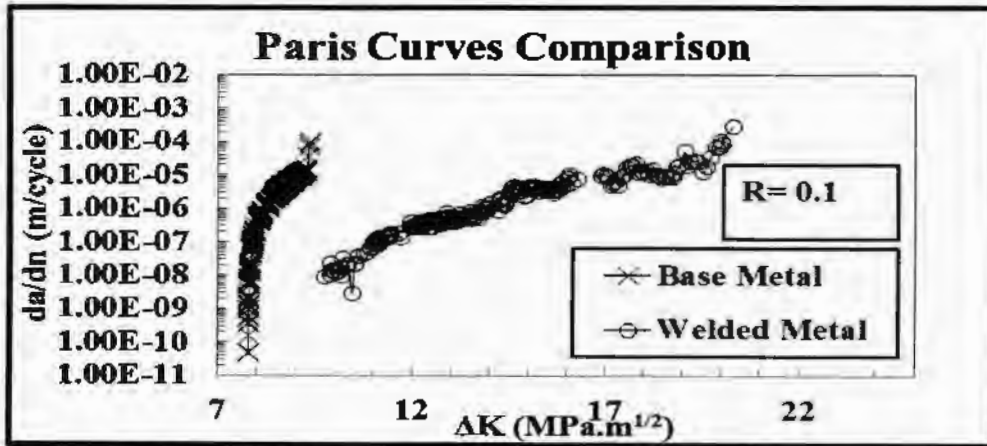
Fig. 5.19 Paris curves comparison obtained from COD gauge

5.11.2 After aging

Comparison of Paris curves for both base metal and welded specimen after natural aging has been shown combined in the Figure 5.20.
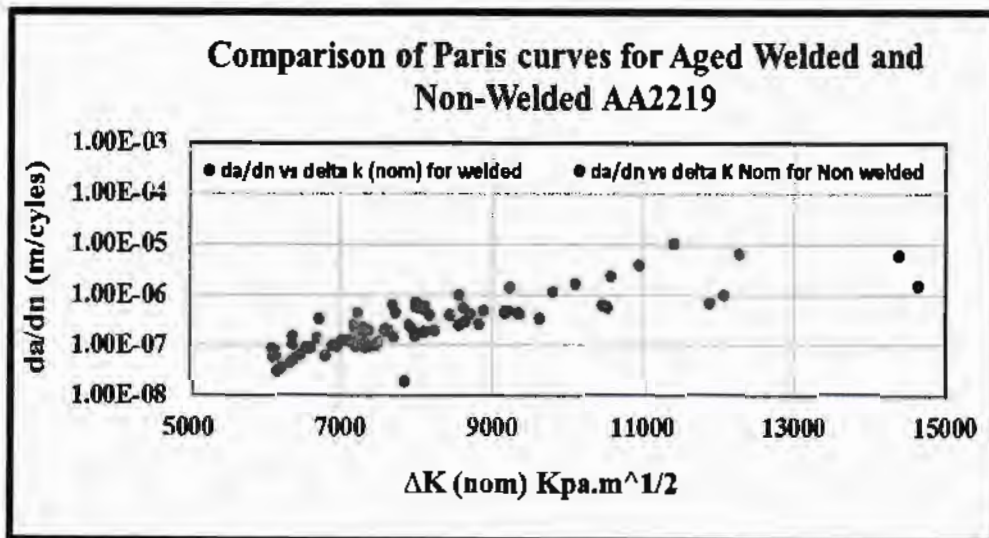
Fig. 5.20 Paris curves comparison obtained from COD gauge after aging

6 *Conclusion and future recommendation*

In this research work, a little effort has been done to investigate the effect of natural aging on TIG welded and non-welded Al-2219-T87. A similar work was performed on the same material and testing parameters but without aging 02 years ago. My work is to compare the results with the already published data of same material and specimen without natural aging condition and draw the conclusion on A lot of work has also been performed previously on artificial aging but no such specific work has yet been done on naturally aged specimens and their comparison with the same specimens without natural aging. Here are some of the main factors which played a vital role in my research work:

> For fatigue crack growth rate study, compact tension (CT) specimens of AA-2219 have been selected and prepared as per ASTM Standard E399. The hest suitable welding technique used for this research is TIG and filler material is AA-2319.

> Hardness test is being performed on hardness tester and microstructure evaluation has been done on metallurgical microscope as well as on Scanning Electron Microscopy (SEM) to examine the mechanical changing in microstructure due to natural aging. The effect of natural aging on different zones of TIG welding has also been investigated.

> All the fatigue testing has becn done on MTS-810 in fracture mechanics and fatigue lab, UET Taxila. During fatigue testing, the load ratio R and room temperature is kept constant.

> After testing, suitable equations are developed corresponding to the CT specimen to show the fatigue data in a reasonable manner.

> From the above equations, graphs are plotted and the results are compared with the previous published data of same specimens before natural aging.

6.1 Conclusion

6.1.1 Before Aging

The results of previous research have been concluded below:

In Chapter No 03, the microstructure evaluation has been done at different welding zones before aging for given specimen. Due to pre-heat treatment of given specimen, the strengthening particles, which are the main source of strength in base metal, are dispersed in the grain. With respect to the strength, most fragile zone is the recrystallized dendritic structure of weld nugget zone (WNZ).

Due to welding, high temperature is produced and due to that, copper is depleted near the weld fusion zone and loses its strength as compared to base metal.

During the modeling of fatigue crack growth behavior before aging, the effect of load ratio R can never be ignored as discussed in chapter no. 04. In the research of without aging, two type of data consolidation techniques, one is based on crack closure and other on mathematical expression, have been introduced to find the fatigue phenomenon. The equations of stress intensity factor and da/dn for a given CT specimen are specific in nature and they cannot be used for any other type of specimens.

In Chapter No. 05, it is concluded that due to TIG welding, though the tensile strength has increased from 50 to 52% of AA2219-T87, but the fatigue crack propagation rate has decreased as compared to the base metal before aging. In short, due to the application of TIG welding, the fatigue strength of AA2219-T87 has increased. From the graphs of stress intensity factor and correction factor of welded and non-welded unaged specimen, it is very clear that relationship has some variations which show the research material has turned into brittle nature after welding.

6.1.2 After Aging:

After the natural aging at room temperature, the specimens with same dimensions and testing parameters have been tested again and the results were discussed and compared with the already published data without aging. These results are as under:

In Chapter No 03, the microstructure evaluation of naturally aged specimen has been done on different zones of welded and non-welded zones using metallurgical microscope as well as SEM. It is clear from the aging of the base metal zone that the grain boundaries are more vivid near the BM/HAZ boundary as compared to the BM zone which is very far from heat source. It might be possible that it's either due to the coagulation of precipitates at the pseudo boundaries or the shrinking of peripheral area of immature grains.

Copper rich boundaries makes HAZ more fragile as compared to non-aged one. This happens due to extra brittleness of the metal at aged boundaries of HAZ. Due to presence of crystallographic disarrangement near foreign particles at grain boundaries, the fatigue strength of this zone is very poor as compared to any other zone investigated in this research.

From the microstructure of aged weld nugget zone, it is observed that the dendritic structure, which is obtained after welding due to segregation of α and θ phase, has been recrystallized completely. The precipitates which are arrested due to the rapid cooling of welding, started to separate out from plain aluminum contents. In WNZ, we have also observed that after aging, the dendrite arms are merged to each other or shifted/matured to grain boundaries. This factor might be responsible of decreasing fatigue strength of this zone.

In Chapter No 05, the dependence of critical stress intensity factor on propagating crack length to specimen width ratio is more prominent in after aging results. It has been observed that critical stress intensity factor dependence is finding itself more reliable after aging as compared to before aging as there is no kink in the middle stream of the curve and the data reinforcement is in harmony as compared to the non-aged base metal. It can easily be concluded that the K dependence is more efficiently predicted in after aging scenarios as compared to the before aging ones.

After natural aging process, the base metal has shown some extra softness against cyclic loading and that is due to the disturbance of alloy balanced percentage or some unusual chemical reaction or mechanical mixtures between the trace elements of the subjected metal.

After aging, the resistance against fatigue crack growth has also increased enormously. The vivid reason of this behavior is the uniform distribution of second phase strengthening particles within the grain and at the grain boundaries. This hindrance in crack propagation is equally available in the case of intergranular as well as trans granular failures. There is another reason of strengthening of aged metal is the maturing of Al_2Cu particles which were available above the eutectics equilibrium points. This phenomenon is responsible for extra availability of strengthening particles per unit volume of the weld metal.

It has also been observed that maximum numbers of cycle are consumed in the intermediate section of the curve which shows that fatigue crack initiation and propagation becomes difficult in aged metals and this factor supports that the uniform distribution of strengthening particles is not only on the surface area which was under examination during microscopy but present three dimensionally in the whole cross section of the joint.

6.2 Future Recommendations

- Determination of effect of changing H/W ratio of specimen on fatigue strength.

- Study of effects of changing R ratio on fatigue strength for different filler weldments.

- Crack opening displacement (COD) investigation for specimens having different weldments.

- Study of different aging time on fatigue crack propagation rate of research material

- Study and comparison of experimental results of this research with simulation results by using Abaqus software package.

- Study of Numerical simulation of COD of TIG welded aluminum alloy using different types of fillers.

- Microstructural investigation of post weld heat treated AA2219 TIG welded using three different type of fillers under different welding conditions.

References

[1]. MUDASERULLAH, R.P., R. RAHMAN, and W. Asghar, Fatigue life estimation of different welding zones of oxy acetylene welded aluminum alloy (AA 5052-H32). Nucleus, 2013. 50(3): p. 261-265.

[2]. Ma, W., et al., Influence of solution heat treatment on mechanical response and fracture behaviour of aluminium alloy sheets: an experimental study. Materials & Design, 2015. 88: p. 1119-1126.

[3]. Tomaszewski, T., J. Sempruch, and T. Piątkowski, Verification of selected models of the size effect based on high-cycle fatigue testing on mini specimens made of EN AW-6063 aluminum alloy. Journal of Theoretical and Applied Mechanics, 2014. 52(4): p. 883-894.

[4]. Jones, R., L. Molent, and S. Barter, Calculating crack growth from small discontinuities in 7050-T7451 under combat aircraft spectra. International Journal of Fatigue, 2013. 55: p. 178-182.

[5]. Hong, Y., et al., Propensities of crack interior initiation and early growth for very-high-cycle fatigue of high strength steels. International Journal of Fatigue, 2014. 58: p. 144-151.

[6]. Wang, Y.L., et al., Effect of retrogression and reaging treatment on the microstructure and fatigue crack growth behavior of 7050 aluminum alloy thick plate. Materials & Design, 2014. 55: p. 857-863.

[7]. Cvijović-Alagić, I., et al., Microstructural morphology effects on fracture resistance and crack tip strain distribution in Ti–6Al–4V alloy for orthopedic implants. Materials & Design, 2014. 53: p. 870-880.

[8]. Aasi, J., et al., Prospects for observing and localizing gravitational-wave transients with Advanced LIGO and Advanced Virgo. Living Reviews in Relativity, 2016. 19.

[9]. Sun, G., et al., Evaluation of defect density, microstructure, residual stress, elastic modulus, hardness and strength of laser-deposited AISI 4340 steel. Acta Materialia, 2015. 84: p. 172-189.

[10]. Martelo, D., A. Mateo, and M. Chapetti, Crack closure and fatigue crack growth near threshold of a metastable austenitic stainless steel. International Journal of Fatigue, 2015. 77: p. 64-77.

[11]. Yao, L., et al., Stress ratio dependence of fibre bridging significance in mode I fatigue delamination growth of composite laminates. Composites Part A: Applied Science and Manufacturing, 2017. 95: p. 65-74.

[12]. Gungor, B., et al., Mechanical and microstructural properties of robotic Cold Metal Transfer (CMT) welded 5083-H111 and 6082-T651 aluminum alloys. Materials & Design (1980-2015), 2014. 54: p. 207-211.

[13]. Hiscocks, J., et al., Formation mechanisms of periodic longitudinal microstructure and texture patterns in friction stir welded magnesium AZ80. Materials Characterization, 2016. 122: p. 22-29.

[14]. Behera, A., Optimization of process parameters in laser welding of dissimilar materials in lap joint configuration using multi-objective Taguchi analysis. 2014.

[15]. Gazizov, M., et al., Effect of equal-channel angular pressing and aging on the microstructure and mechanical properties of an Al-Cu-Mg-Si alloy. The Physics of Metals and Metallography, 2015. 116(7): p. 718-729.

[16]. Peng, D., et al., Effects of aging treatment and heat input on the microstructures and mechanical properties of TIG-welded 6061-T6 alloy joints. International Journal of Minerals, Metallurgy, and Materials, 2013. 20(3): p. 259-265.

[17]. Liu, H. and X. Feng, Effect of post-processing heat treatment on microstructure and microhardness of water-submerged friction stir processed 2219-T6 aluminum alloy. Materials & Design, 2013. 47: p. 101-105.

[18]. Ding, J.-k., et al., Effect of post weld heat treatment on properties of variable polarity TIG welded AA2219 aluminium alloy joints. Transactions of Nonferrous Metals Society of China, 2014. 24(5): p. 1307-1316.

[19]. Gao, H., et al., Stress relaxation due to ultrasonic impact treatment on multi-pass welds. Science and Technology of Welding and Joining, 2014. 19(6): p. 505-513.

[20]. Pare, V. and K.N. Jonnalagadda, Thermo-mechanical behavior of AA-2219 and AA-2195 at high strain rates, in Dynamic Behavior of Materials, Volume 1. 2015, Springer. p. 241-247.

[21]. Savaidis, G. and M. Malikoutsakis, Advanced notch strain based calculation of S–N curves for welded components. International Journal of Fatigue, 2016. 83: p. 84-92.

[22]. Venkatasubramanian, G., et al., Inhibitive effect of Ce (III) and La (III) cations for AA2219 aluminium alloy corrosion in sodium chloride medium. Materials Chemistry and Physics, 2014. 148(1): p. 262-275.

[23]. Murty, S.N., S.K. Manwatkar, and P.R. Narayanan, Role of Metallographic Analysis in the Identification of Location of Crack Initiation in a Burst Tested AA 2219 Propellant Tank. Metallography, Microstructure, and Analysis, 2015. 4(5): p. 392-402.

[24]. Lei, X., et al., Tungsten inert gas and friction stir welding characteristics of 4-mm-thick 2219-T87 plates at room temperature and− 196° C. Journal of Materials Engineering and Performance, 2014. 23(6): p. 2149-2158.

[25]. Calignano, F., Design optimization of supports for overhanging structures in aluminum and titanium alloys by selective laser melting. Materials & Design, 2014. 64: p. 203-213.

[26]. Dursun, T. and C. Soutis, Recent developments in advanced aircraft aluminium alloys. Materials & Design, 2014. 56: p. 862-871.

[27]. Ruggieri, C. and R.H. Dodds, An engineering methodology for constraint corrections of elastic–plastic fracture toughness–Part I: A review on probabilistic models and exploration of plastic strain effects. Engineering Fracture Mechanics, 2015. 134: p. 368-390.

[28]. Lynch, S., et al., Fracture toughness and fracture modes of aerospace aluminum–lithium alloys, in Aluminum-lithium Alloys. 2014, Elsevier. p. 415-455.

[29]. Wanhill, R., Aerospace applications of aluminum–lithium alloys, in Aluminum-lithium Alloys. 2014, Elsevier. p. 503-535.

[30]. Jae-Ho, J., et al., Effect of solution treatment and artificial aging on microstructure and mechanical properties of Al–Cu alloy. Transactions of Nonferrous Metals Society of China, 2013. 23(3): p. 631-635.

[31]. AN, L.-h., et al., Effect of pre-deformation on microstructure and mechanical properties of 2219 aluminum alloy sheet by thermomechanical treatment. Transactions of nonferrous metals society of China, 2012. 22: p. s370-s375.

[32]. Zhu, Z., et al., Effect of post weld heat treatment on the microstructure and corrosion behavior of AA2219 aluminum alloy joints welded by variable polarity tungsten inert gas welding. Materials & Design (1980-2015), 2015. 65: p. 1075-1082.

[33]. Cao, L., P.A. Rometsch, and M.J. Couper, Clustering behaviour in an Al–Mg–Si–Cu alloy during natural ageing and subsequent under-ageing. Materials Science and Engineering: A, 2013. 559: p. 257-261.

[34]. Takaki, Y., et al., Effects of Natural Aging on Bake Hardening Behavior of Al–Mg–Si Alloys with Multi-Step Aging Process. Materials Transactions, 2014. 55(8): p. 1257-1265.

[35]. Arunkumar, S., et al., Comparative study on transverse shrinkage, mechanical and metallurgical properties of AA2219 aluminium weld joints prepared by gas tungsten arc and gas metal arc welding processes. Defence technology, 2015. 11(3): p. 262-268.

[36]. Trdan, U., M. Skarba, and J. Grum, Laser shock peening effect on the dislocation transitions and grain refinement of Al–Mg–Si alloy. Materials Characterization, 2014. 97: p. 57-68.

[37]. Shaterani, P., et al., The second phase particles and mechanical properties of 2124 aluminum alloy processed by accumulative back extrusion. Materials & Design, 2014. 58: p. 535-542.

[38]. Azad, B. and E. Borhani, The Effect of Al2Cu Precipitate Size on Microstructure and Mechanical Properties of Al-2 wt.% Cu Alloys Fabricated by ARB. Journal of Materials Engineering and Performance, 2015. 24(12): p. 4789-4796.

[39]. Krishnan, M.M. and K. Marimuthu, Effect of post-weld heat treatment on dissimilar friction stir welded AA6063 and A319 aluminium alloys. International Journal of Materials Research, 2014. 105(5): p. 507-511.

[40]. Zhang, X., et al., Investigation of the de-alloying behaviour of θ-phase (Al 2 Cu) in AA2024-T351 aluminium alloy. Corrosion Science, 2016. 108: p. 85-93.

[41]. Ahn, J., et al., Effect of filler metal feed rate and composition on microstructure and mechanical properties of fibre laser welded AA 2024-T3. Journal of Manufacturing Processes, 2017. 25: p. 26-36.

[42]. Karthik, J., D.M. Kumar, and J.R.R. Chowdary, Assessment and Comparison of Fatigue Life for Heavy Truck Wheel Rim Rnder Fully Reverse Loading for Aluminium Alloys. International Journal of Applied Science and Engineering, 2015. 13(1): p. 69-79.

[43]. Shanyavskiy, A., Very-High-Cycle-Fatigue of in-service air-engine blades, compressor and turbine. Science China Physics, Mechanics and Astronomy, 2014. 57(1): p. 19-29.

[44]. Gludovatz, B., et al., A fracture-resistant high-entropy alloy for cryogenic applications. Science, 2014. 345(6201): p. 1153-1158.

[45]. Radaj, D., State-of-the-art review on the local strain energy density concept and its relation to the J-integral and peak stress method. Fatigue & Fracture of Engineering Materials & Structures, 2015. 38(1): p. 2-28.

[46]. Olakanmi, E.O.t., R. Cochrane, and K. Dalgarno, A review on selective laser sintering/melting (SLS/SLM) of aluminium alloy powders: Processing, microstructure, and properties. Progress in Materials Science, 2015. 74: p. 401-477.

[47]. Riemer, A., et al., On the fatigue crack growth behavior in 316L stainless steel manufactured by selective laser melting. Engineering Fracture Mechanics, 2014. 120: p. 15-25.

[48]. Kratochvíl, P., et al., Evaluation of Solid-Solution Hardening of Fe-27 at. pct Al by Vanadium and Comparison to Precipitation Strengthening by Vanadium Carbides. Metallurgical and Materials Transactions A, 2015. 46(11): p. 5091-5094.

[49]. Antunes, F., L. Correia, and A. Ramalho, A parameter for quantitative analysis of plasticity induced crack closure. International Journal of Fatigue, 2015. 71: p. 87-97.

[50]. Wei, L., et al., Influence of grain structure and crystallographic orientation on fatigue crack propagation behavior of 7050 alloy thick plate. International Journal of Fatigue, 2014. 66: p. 55-64.

[51]. Designation, A., E399-90. Standard test method for plane-strain fracture toughness of metallic materials. 1991 Annual Book of ASTM Standards, 1997. 3: p. 485-51.

[52]. Shah, S.M.R., Investigation of crack propagation in X38CrMoV5 tool steel at room temperature and 600° C on small scale specimens. 2010, Université de Toulouse, Université Toulouse III-Paul Sabatier.

[53]. Raabe, D., et al., Grain boundary segregation engineering in metallic alloys: A pathway to the design of interfaces. Current Opinion in Solid State and Materials Science, 2014. 18(4): p. 253-261.

[54]. Zhang, X., et al., Investigation on effect of laser shock processing on fatigue crack initiation and its growth in aluminum alloy plate. Materials & Design (1980-2015), 2015. 65: p. 425-431.

[55]. Sultan, A., et al., Numerical simulation and experimental verification of CMOD in SENT specimen: Application on FCGR of welded tool steel. Acta Metallurgica Sinica (English Letters), 2013. 26(1): p. 92-96.